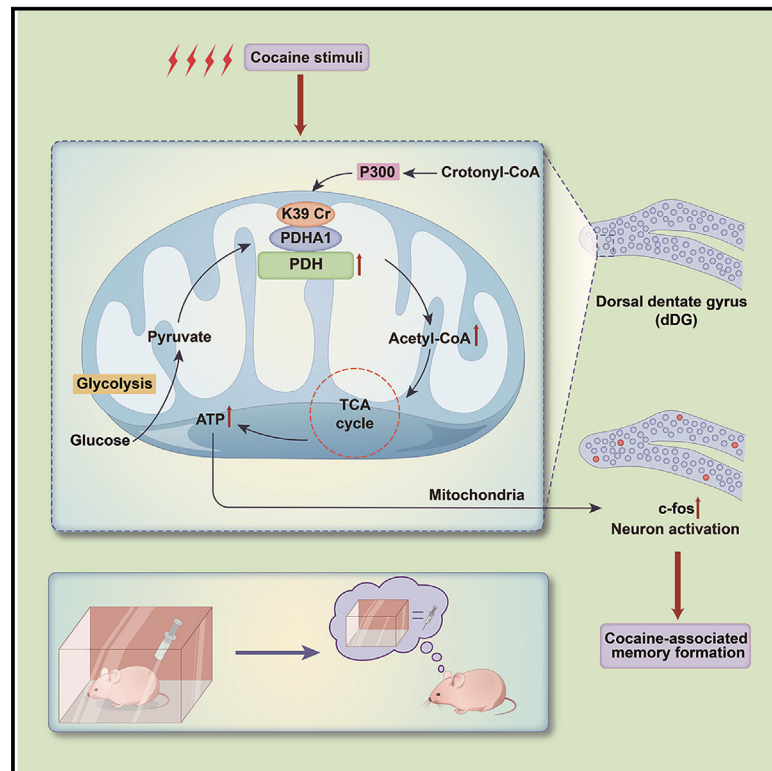


Pyruvate dehydrogenase complex E1 subunit α crotonylation modulates cocaine-associated memory through hippocampal neuron activation

Graphical abstract



Authors

Hongchun Li, Xiaoyu Liuha, Rong Chen, ..., Jingwei Tian, Yinglan Zhao, Xiaobo Cen

Correspondence

xbcen@scu.edu.cn

In brief

Li et al. report that cocaine markedly increases the level of PDHA1 crotonylation at the K39 residue in the dorsal dentate gyrus (dDG) through P300 catalysis. Crotonylated PDHA1 promotes pyruvate metabolism by activating PDH to increase ATP production, thus providing energy for hippocampal neuronal activation and promoting cocaine-associated memory recall.

Highlights

- Kcr protein levels are elevated in the hippocampal dDG after cocaine CPP training
- PDHA1 K39 Cr promotes pyruvate metabolism by activating PDH to increase ATP
- PDHA1 Cr enhances cocaine-associated memory by providing ATP for neuronal activation



Article

Pyruvate dehydrogenase complex E1 subunit α crotonylation modulates cocaine-associated memory through hippocampal neuron activation

Hongchun Li,¹ Xiaoyu Liuha,² Rong Chen,¹ Yuzhou Xiao,¹ Wei Xu,^{3,4} Yuanyi Zhou,¹ Lin Bai,⁵ Jie Zhang,⁵ Yue Zhao,¹ Ying Zhao,¹ Liang Wang,¹ Feng Qin,¹ Yaxing Chen,¹ Shuang Han,¹ Qingfan Wei,¹ Shu Li,¹ Dingwen Zhang,¹ Qian Bu,^{1,6} Xiaojie Wang,¹ Linhong Jiang,¹ Yanping Dai,¹ Ni Zhang,¹ Weihong Kuang,¹ Meng Qin,¹ Hongbo Wang,² Jingwei Tian,² Yinglan Zhao,¹ and Xiaobo Cen^{1,7,*}

¹Mental Health Center and Center for Preclinical Safety Evaluation of Drugs, State Key Laboratory of Biotherapy, West China Hospital, Sichuan University, Chengdu 610041, China

²Ministry of Education, Collaborative Innovation Center of Advanced Drug Delivery System and Biotech Drugs in Universities of Shandong, Yantai University, Yantai 264005, China

³Shenzhen Key Laboratory of Drug Addiction, Shenzhen Neher Neural Plasticity Laboratory, the Brain Cognition and Brain Disease Institute, Shenzhen Institute of Advanced Technology, Chinese Academy of Sciences, Shenzhen 518055, China

⁴Faculty of Life and Health Sciences, Shenzhen University of Advanced Technology, Shenzhen 518055, China

⁵Histology and Imaging Platform, Core Facilities of West China Hospital, Sichuan University, Chengdu 610041, China

⁶West China-Frontier PharmaTech Co., Ltd., Chengdu 610041, China

⁷Lead contact

*Correspondence: xbcen@scu.edu.cn

<https://doi.org/10.1016/j.celrep.2024.114529>

SUMMARY

Neuronal activation is required for the formation of drug-associated memory, which is critical for the development, persistence, and relapse of drug addiction. Nevertheless, the metabolic mechanisms underlying energy production for neuronal activation remain poorly understood. In the study, a large-scale proteomics analysis of lysine crotonylation (Kcr), a type of protein posttranslational modification (PTM), reveals that cocaine promoted protein Kcr in the hippocampal dorsal dentate gyrus (dDG). We find that Kcr is predominantly discovered in a few enzymes critical for mitochondrial energy metabolism; in particular, pyruvate dehydrogenase (PDH) complex E1 subunit α (PDHA1) is crotonylated at the lysine 39 (K39) residue through P300 catalysis. Crotonylated PDHA1 promotes pyruvate metabolism by activating PDH to increase ATP production, thus providing energy for hippocampal neuronal activation and promoting cocaine-associated memory recall. Our findings identify Kcr of PDHA1 as a PTM that promotes pyruvate metabolism to enhance neuronal activity for cocaine-associated memory.

INTRODUCTION

Drug-associated memory is critical for the development, persistence, and relapse of drug addiction. Its formation requires neuronal activity in the hippocampus,¹ especially the dorsal dentate gyrus (dDG),² which is crucial for drug-induced changes in neuronal morphology and excitability, synaptic plasticity, and neuronal circuits.³ These adaptive changes encode the associations between drugs and contextual cues necessary for drug-associated memory formation.

Neuronal activation is a highly energy-demanding process that strongly relies on mitochondria for neuronal pyruvate consumption-induced ATP production.⁴ Cocaine-associated memory encoding is regulated by the activation of hippocampal neurons,² which requires mitochondrial-regulated energy production, the promotion of localized protein synthesis within dendrites, and the activation of gene transcription.^{4,5} Currently, several mechanisms have been proposed to elucidate how cocaine regulates

hippocampal neuron activity, such as by promoting dendritic spine formation,⁶ enhancing hippocampal long-term potentiation⁷ and neurotransmitter transmission,^{8,9} and modulating neurotrophic or inflammatory factor production.¹⁰ More recently, reprogrammed energy metabolism was shown to be associated with drug-induced neuronal activity in the brain.¹¹ However, how cocaine modulates neuronal activity through neuroenergetics driven by mitochondrial energy metabolism remains largely unknown.

Lysine crotonylation (Kcr) is a newly identified posttranslational modification (PTM) with key roles in various important regulatory pathways.¹² During Kcr, crotonyl-coenzyme A (CoA), the precursor of Kcr, is utilized by crotonyltransferases as a cofactor.¹³ Through mass spectrometry (MS)-based proteomics, the endogenous crotonylation (Cr) of proteins has increasingly been identified, and in particular, numerous nonhistone Kcr proteins have been discovered.^{14–17} Some key enzymes in metabolic pathways have been shown to undergo



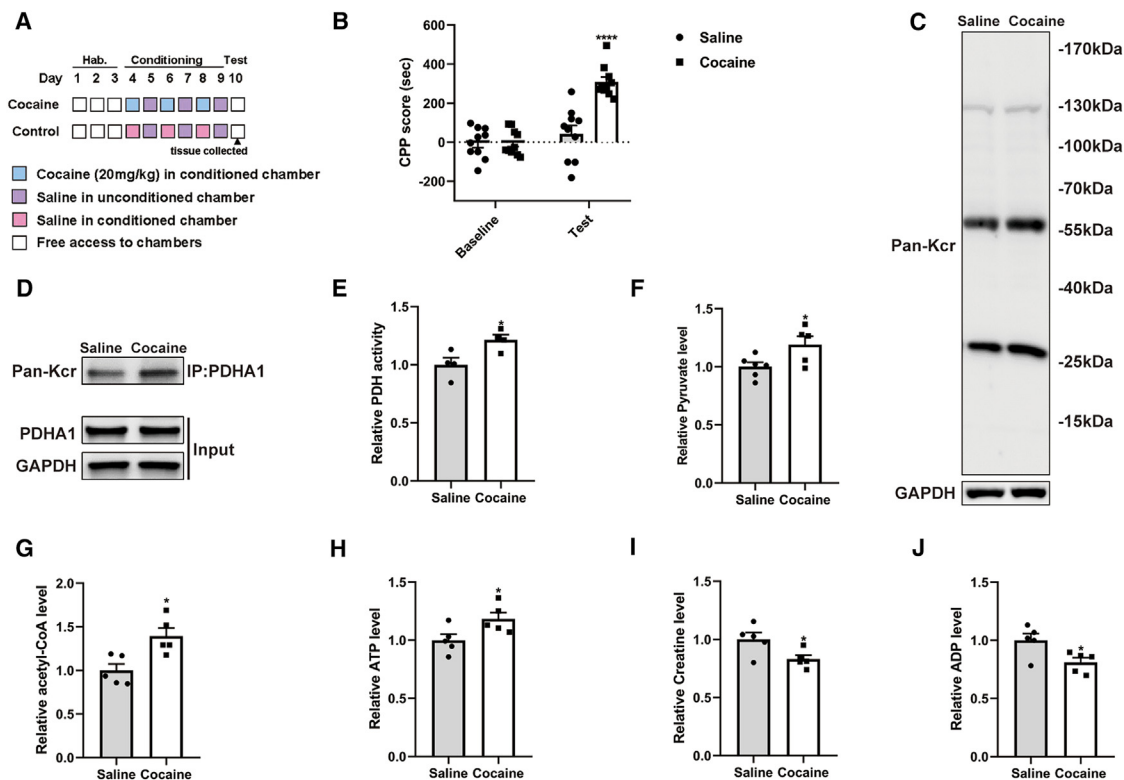


Figure 1. Lysine crotonylome in the dDG during cocaine-associated memory formation

(A) Schematic of the experimental workflow for mouse cocaine CPP training.
 (B) The CPP score significantly increased in the cocaine group after CPP training ($n = 10$ per group).
 (C) Western blotting analysis showing the level of Pan-Kcr in the dDG after CPP training ($n = 6$ per group).
 (D) Western blotting analysis showing the level of endogenous PDHA1 Kcr in the dDG after CPP training ($n = 3$ per group).
 (E–H) PDH activity and pyruvate, acetyl-CoA, and ATP levels were increased in the dDG after CPP training (PDH activity: $n = 4$ per group; pyruvate: $n = 6$ for the saline group, $n = 5$ for the cocaine group; acetyl-CoA: $n = 5$ per group; ATP: $n = 5$ per group).
 (I and J) The levels of creatine and ADP were decreased in the dDG after CPP training (creatine: $n = 5$ per group; ADP: $n = 5$ per group).
 The data are the means \pm SEMs. Unpaired t test, * $p < 0.05$ and **** $p < 0.0001$. Hab, habituation.

Kcr and subsequently affect the energy metabolism homeostasis of cells,^{18,19} suggesting a crucial link between the Kcr of metabolic enzymes and energy metabolism regulation. However, whether Kcr occurs in enzymes involved in mitochondrial energy metabolism to activate hippocampal neurons is unknown.

The pyruvate dehydrogenase (PDH) complex is a key rate-limiting enzyme complex involved in maintaining the tricarboxylic acid (TCA) cycle in mitochondria; this complex converts pyruvate to acetyl-CoA and thereby links glycolysis to oxidative phosphorylation to control ATP production.²⁰ The PDH complex is composed of the rate-limiting E1 subunit (catalytic subunit α [PDHA1], the regulatory subunit β) and the E2 and E3 subunits, and the integrity of this complex is critical for PDH activity.²¹ Currently, PDH activity is mainly modulated by two types of PTMs of PDHA1, phosphorylation and acetylation, and thus regulates mitochondrial energy production in cells.^{22–24} Whether other types of PTMs exist in PDHA1, especially in hippocampal neurons, is unknown.

In the present study, through a quantitative proteomics approach, we profiled the global crotonylome of the hippocampal dDG of mice conditioned by cocaine. We discovered that

cocaine markedly increased the level of PDHA1 Cr at the K39 residue in the dDG, thus activating PDH and promoting both pyruvate metabolism and ATP production, which are necessary for hippocampal neuron activation. Our findings connect Kcr modification of PDHA1, a critical metabolic enzyme in glucose catabolism, with cocaine-associated memory.

RESULTS

Global crotonylome of the hippocampal dDG during cocaine-associated memory formation

The conditioned place preference (CPP) paradigm, an associative memory paradigm in which a drug reward is linked with environmental cues, is widely used to assess the formation of drug-associated memory.^{1,2} The timeline of the cocaine CPP training procedure is shown in Figure 1A. During habituation to the CPP apparatus, neither group showed a side preference. However, cocaine significantly increased the CPP score after training (Figure 1B; $t_{(18)} = 5.373$, $p < 0.001$). Because Kcr is involved in pathways that regulate diverse cellular functions,²⁵ especially energy metabolism,^{18,19} we explored whether protein Kcr occurs in the

dDG during cocaine-associated memory formation. Interestingly, western blotting analysis revealed that cocaine increased the total level of protein Kcr in the dDG after CPP training (Figure 1C). We next performed label-free analysis of the crotonylome in the dDG in saline- and cocaine-treated mice after CPP training. The analysis revealed 9,637 Kcr sites in 3,038 proteins in the saline group and 9,734 Kcr sites in 3,066 proteins in the cocaine group. Because some Kcr sites of proteins overlapped, a total of 14,072 Kcr sites across 3,128 proteins were identified in these two groups, and 10,665 Kcr sites from 2,593 proteins were quantified (Table S1).

Quantitative analysis of the dDG crotonylome

We next quantified the changes in the Kcr levels of total proteins in the mouse dDG during cocaine-associated memory formation. The cutoff values for significant changes in Kcr levels between cocaine- and saline-treated mice were set to greater than 1.5 or less than 0.67. The Kcr increased at 588 sites but decreased at 433 sites in the dDG after cocaine CPP training (Figures S1A and S1B). Notably, among the protein residues with significant alterations in Kcr levels, 62 sites in 61 proteins were crotonylated only in cocaine-treated mice, and 89 sites in 87 proteins were completely decrotonylated (Table S1). Interestingly, Kyoto Encyclopedia of Genes and Genomes pathway analysis revealed that those proteins with Kcr levels were mainly involved in starch and sucrose metabolism (Figure S1C). In addition, among the proteins with altered Kcr levels, those with increased Kcr levels were dominantly enriched in glycolysis or gluconeogenesis, whereas those with decreased Kcr levels were enriched in pathogenic *Escherichia coli* infection (Figures S1D and S1E). Considering that these crotonylated enzymes play important roles in the regulation of metabolic homeostasis,¹⁸ we speculated that those enzymes with increased Kcr levels may be associated with the effect of cocaine. To prove this link, a protein-protein interaction network was generated and visualized using Cytoscape software based on the Search Tool for the Retrieval of Interacting Genes/Proteins database. As a result, we focused on metabolism-regulating enzymes that are enriched in the TCA cycle as well as glycolysis and gluconeogenesis (Figure S1F). Considering the key role of energy metabolism and the dendritic structural remodeling of hippocampal neurons in drug addiction,^{26,27} among the proteins with increased Kcr levels, we selected PDHA1²⁸ and phosphofructokinase muscle (PFKM),²⁹ the two key enzymes in energy metabolism, as well as β -adducin,³⁰ an important regulator of dendrite structural remodeling, and investigated the effect of Kcr on the activities and functions of these proteins.

PDHA1 Kcr is enhanced during cocaine-associated memory formation

We first validated whether PDHA1, PFKM, and β -adducin were crotonylated by immunoprecipitation with antibodies against these proteins followed by immunoblotting with an anti-pan Kcr antibody. Western blotting analysis revealed that the levels of these proteins in the dDG of cocaine-treated mice did not differ from those in the dDG of saline-treated mice. Notably, the Kcr level of PDHA1 was markedly increased; nevertheless,

the Kcr levels of both β -adducin and PFKM were not altered (Figures 1D, S2A, and S2B).

To investigate whether the increase in the dDG Kcr of PDHA1 was specific to cocaine memory, we investigated two other reward paradigms, home cage cocaine injection and food CPP. In the first paradigm, mice were injected with cocaine but not exposed to cocaine-associated cues (Figures S3A and S3B). In the latter paradigm, food-associated memory was established in the mice by exposure to a palatable food reward in the absence of cocaine (Figures S3D and S3E; $t_{(16)} = 2.555$, $p < 0.05$). The level of PDHA1 Kcr in the dDG was not altered in the mice subjected to either of these two paradigms (Figures S3C and S3F). In addition, when mice were subjected to a locomotor test in the absence of cocaine-associated contextual stimuli, the level of PDHA1 Kcr was also not altered after cocaine injection for 7 consecutive days (Figures S3G–S3I; treatment: $F_{(7, 112)} = 8.696$, $p < 0.0001$; time: $F_{(1, 112)} = 330.8$, $p < 0.0001$; interaction: $F_{(7, 112)} = 11.55$, $p < 0.0001$). Finally, the mice were conditioned to a context in which they received 3 foot shocks, and fear behavior was quantified in the same context after training. Similarly, the level of PDHA1 Kcr was also not altered after the contextual fear conditioning test (Figures S3J–S3L; $t_{(14)} = 7.92$, $p < 0.0001$). Collectively, these results suggested that cocaine can promote PDHA1 Kcr in the dDG, which may be correlated with cocaine-associated memory.

Because PDH activity is regulated by PDHA1 PTMs, we speculated that Kcr may be a PTM of PDHA1 that affects PDH activity. To this end, we measured PDH activity in the dDG after cocaine CPP training. The results showed that PDH activity was significantly increased in the dDG of mice subjected to the cocaine CPP paradigm (Figure 1E; $t_{(6)} = 2.905$, $p < 0.05$). Consistent with this result, the levels of pyruvate, acetyl-CoA, and ATP were also markedly increased in the dDG (Figures 1F–1H; pyruvate: $t_{(6)} = 2.476$, $p < 0.05$; acetyl-CoA: $t_{(6)} = 3.32$, $p < 0.05$; ATP: $t_{(6)} = 2.452$, $p < 0.05$), whereas the levels of creatine and ADP were decreased (Figures 1I and 1J; creatine: $t_{(6)} = 2.528$, $p < 0.05$; ADP: $t_{(6)} = 2.656$, $p < 0.05$). These data suggested that PDHA1 Kcr may promote pyruvate metabolism through oxidative phosphorylation in the dDG, thus promoting the production of both acetyl-CoA and ATP after cocaine CPP training.

To explore the direct effect of PDHA1 Kcr on PDH activity, we treated HT22 cells (a mouse hippocampal cell line) with croconic acid sodium (NaCr) at different concentrations (0, 5, 10, and 20 mM) for 24 h *in vitro*. NaCr is able to increase protein Kcr, most likely through the conversion of NaCr to crotonyl-CoA in cells.^{31,32} We found that 20 mM NaCr significantly increased the level of Pan-Kcr in HT22 cells (Figure S4A), indicating that NaCr was capable of directly driving Kcr in HT22 cells. Thus, we selected 20 mM as the treatment concentration of NaCr for subsequent cell experiments. Next, we immunoprecipitated PDHA1 from NaCr-treated and -untreated cells and analyzed the Kcr of PDHA1 with a Pan-Kcr antibody. Western blotting analysis indicated that the level of PDHA1 Kcr was significantly increased in NaCr-treated cells even though the total PDHA1 expression level did not change (Figure S4B). We further analyzed PDH activity and energy production and observed significantly increased PDH activity in the NaCr-treated cells,

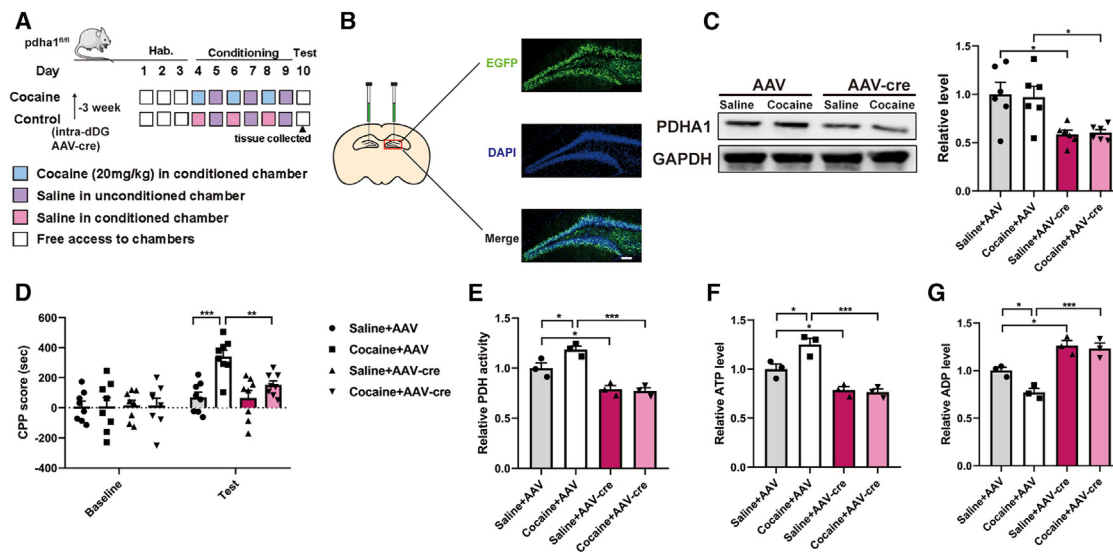


Figure 2. Inhibition of PDHA1 in dDG neurons inhibits cocaine-associated memory

(A) Schematic representation of the experimental workflow for mouse cocaine CPP training.

(B) Representative images of AAV-cre-EGFP expression in the dDG (green) and DAPI staining (blue). Scale bar, 100 μ m.

(C) Western blotting analysis showing the level of PDHA1 in the dDG after CPP training ($n = 6$ per group).

(D) Inhibition of neuronal PDHA1 expression in the dDG decreased cocaine CPP scores ($n = 8$ per group).

(E and F) The levels of PDH activity and ATP were decreased after the inhibition of neuronal PDHA1 expression in the dDG during cocaine-associated memory ($n = 3$ per group).

(G) The level of ADP was increased after the inhibition of neuronal PDHA1 expression in the dDG during cocaine-associated memory formation ($n = 3$ per group). The data are the means \pm SEMs. One-way or two-way ANOVA, * $p < 0.05$, ** $p < 0.01$, and *** $p < 0.001$. Hab, habituation.

and this increase was accompanied by significantly elevated levels of pyruvate, acetyl-CoA, and ATP but reduced levels of creatine and ADP (Figures S4C–S4H; PDH activity: $t_{(6)} = 2.844$, $p < 0.05$; pyruvate: $t_{(6)} = 2.826$, $p < 0.05$; acetyl-CoA: $t_{(6)} = 3.457$, $p < 0.05$; ATP: $t_{(4)} = 3.144$, $p < 0.05$; creatine: $t_{(6)} = 2.804$, $p < 0.05$; ADP: $t_{(6)} = 3.303$, $p < 0.05$). These results showed that NaCr is able to promote both cellular PDHA1 Kcr and PDH activity, thus increasing cellular acetyl-CoA and ATP production.

PDHA1 is necessary for PDH activity and energy production in hippocampal neurons

Because we observed that PDHA1 Kcr can modulate PDH activity and ATP production, as described above, we assessed whether PDHA1, a critical catalytic component of the PDH complex, functions in regulating PDH activity and ATP production in hippocampal neurons. To this end, by transfecting HT22 cells with PDHA1 short hairpin RNA (shRNA), we knocked down PDHA1 expression (Figure S4I; $t_{(4)} = 8.478$, $p < 0.01$). Importantly, PDH activity was markedly reduced (Figure S4J; $t_{(4)} = 7.527$, $p < 0.01$), the levels of acetyl-CoA and ATP were consistently decreased (Figures S4K and S4L; acetyl-CoA: $t_{(4)} = 7.527$, $p < 0.01$; ATP: $t_{(4)} = 5.299$, $p < 0.01$), and the ADP level was increased (Figure S4M; $t_{(4)} = 5.565$, $p < 0.01$) in the HT22 cells with PDHA1 deficiency.

To further confirm whether PDHA1 in dDG neurons is necessary for cocaine-associated memory formation, the *PDHA1* gene was conditionally knocked out in the dDG neurons of mice, and these mice were subjected to neurobehavioral tests. To conditionally knock out *PDHA1*, AAV-CaMKII-cre was stereo-

tactically microinfused into the dDG of *PDHA1^{fl/fl}* mice before CPP training (Figure 2A), and cre expression was visualized via EGFP (Figure 2B). As expected, the PDHA1 level was decreased in the mouse dDG (Figure 2C; $F_{(3,20)} = 6.663$, $p < 0.05$), and the CPP score was significantly decreased in the *PDHA1* knockout (KO) mice after cocaine CPP training (Figure 2D; treatment $F_{(1,56)} = 22.97$, $p < 0.0001$; time $F_{(3,56)} = 4.458$, $p = 0.0071$; interaction $F_{(3,56)} = 4.646$, $p = 0.0057$). Consistently, PDH activity and ATP levels in the dDG were decreased and ADP levels were increased in *PDHA1* KO mice (Figures 2E–2G; PDH activity: $F_{(3,8)} = 23.34$, $p < 0.001$; ATP: $F_{(3,8)} = 23.51$, $p < 0.001$; ADP: $F_{(3,8)} = 23.30$, $p < 0.001$). Taken together, these results show that PDHA1 in dDG neurons is necessary for PDH activity and ATP production and that the inhibition of PDHA1 in dDG neurons disrupts cocaine-associated memory, possibly by suppressing PDH activity and energy production.

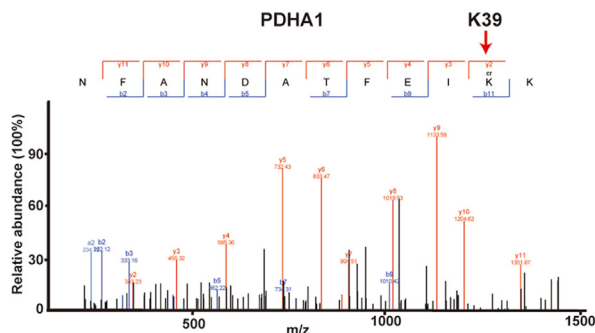
PDHA1 is highly crotonylated at the K39 site during cocaine-associated memory formation

We continued to investigate the role of PDHA1 Kcr in the dDG in cocaine-associated memory formation. First, a total of ten crotonylated lysine residues were identified in PDHA1 through liquid chromatography-tandem MS analysis; notably, the K39 residue was specifically crotonylated by cocaine (Figure 3A), and the other nine residues showed no changes in Kcr levels (Table S1). The MS data further supported this finding, which showed a mass shift at the K39 residue of PDHA1 (Figure 3B). To confirm that the K39 residue of PDHA1 was specifically crotonylated, we generated PDHA1 K39 Cr-specific antibodies,

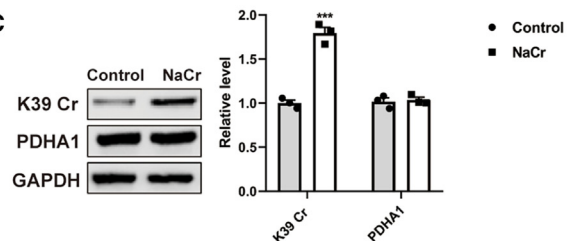
A

Protein accession	Position	Regulated Type	Amino acid	Gene name	Score	Charge	Mass error [ppm]	S1	S2	S3	C1	C2	C3	Subcellular localization
P35486	39	Up	K	Pdha1	88.734	2	-6.0194	/	/	/	0.999371634	0.83559246	1.165035907	mitochondria

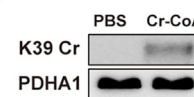
B



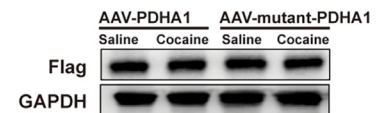
C



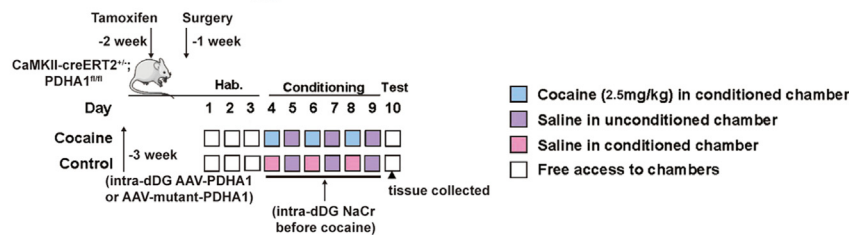
D



F



E



G

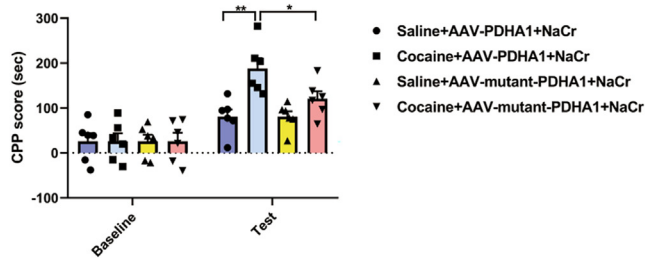


Figure 3. PDHA1 is highly Kcr at K39

(A) Proteomic analysis of the specific Cr of K39 in PDHA1 after cocaine CPP training ($n = 3$ per group). (B) Mass spectrometry analysis of PDHA1-derived peptides Cr at K39. (C) Western blotting analysis showing the levels of K39 Cr and PDHA1 in HT22 cells treated with NaCr ($n = 3$ per group). (D) Western blotting analysis showing the level of K39 Cr in the recombinant PDHA1 protein after Cr-CoA treatment. (E) Schematic diagram of the experimental design for AAV and tamoxifen injection, brain stereotaxic surgery, NaCr administration, and cocaine CPP. (F) Western blotting analysis showing the level of FLAG in the dDG after CPP training ($n = 6$ per group). (G) Promoting PDHA1 K39 Cr in the dDG significantly increased CPP scores ($n = 6$ per group). The data are the means \pm SEMs. One-way or two-way ANOVA, * $p < 0.05$, ** $p < 0.01$, and *** $p < 0.001$. Hab, habituation.

the specificity of which was validated by dot blot assays using crotonylated and noncrotonylated peptides (Figures S5A–S5D). We then transfected HT22 cells with a lentivirus (LV) expressing FLAG-tagged PDHA1 or mutant PDHA1 (K39 mutated to A39); an LV expressing FLAG-tagged PDHA1 was used as a control. FLAG protein from cells was enriched by FLAG beads through immunoprecipitation, and an immunoblotting analysis with a PDHA1 K39 Cr-specific antibody was then performed. We found that the level of PDHA1 K39 Cr was markedly increased in HT22 cells treated with NaCr (20 mM) for 24 h; however, mutation of PDHA1 (K39 mutated to A39) abolished this effect (Figure S5E). Finally, we further assessed whether the antibody we generated could target PDHA1 acetylated at K39. However, the level of

PDHA1 K39 Cr did not change in HT22 cells treated with acetic acid sodium (NaAc, 20 mM) for 24 h (Figure S5F). These data further showed the specificity of the antibody targeting PDHA1 K39 Cr.

We next measured the level of endogenous PDHA1 K39 Cr in HT22 cells after NaCr treatment. NaCr significantly increased the level of K39 Cr in HT22 cells but did not change the level of PDHA1 (Figure 3C; K39 Cr $t_{(4)} = 10.78$, $p < 0.001$), suggesting that NaCr can directly promote PDHA1 K39 Cr. To further prove this finding, we performed an *in vitro* catalytic activity test in which recombinant PDHA1 was incubated with crotonoyl-CoA at 37°C for 2 h. Importantly, crotonoyl-CoA markedly increased the level of PDHA1 K39 Cr in the absence of any potential

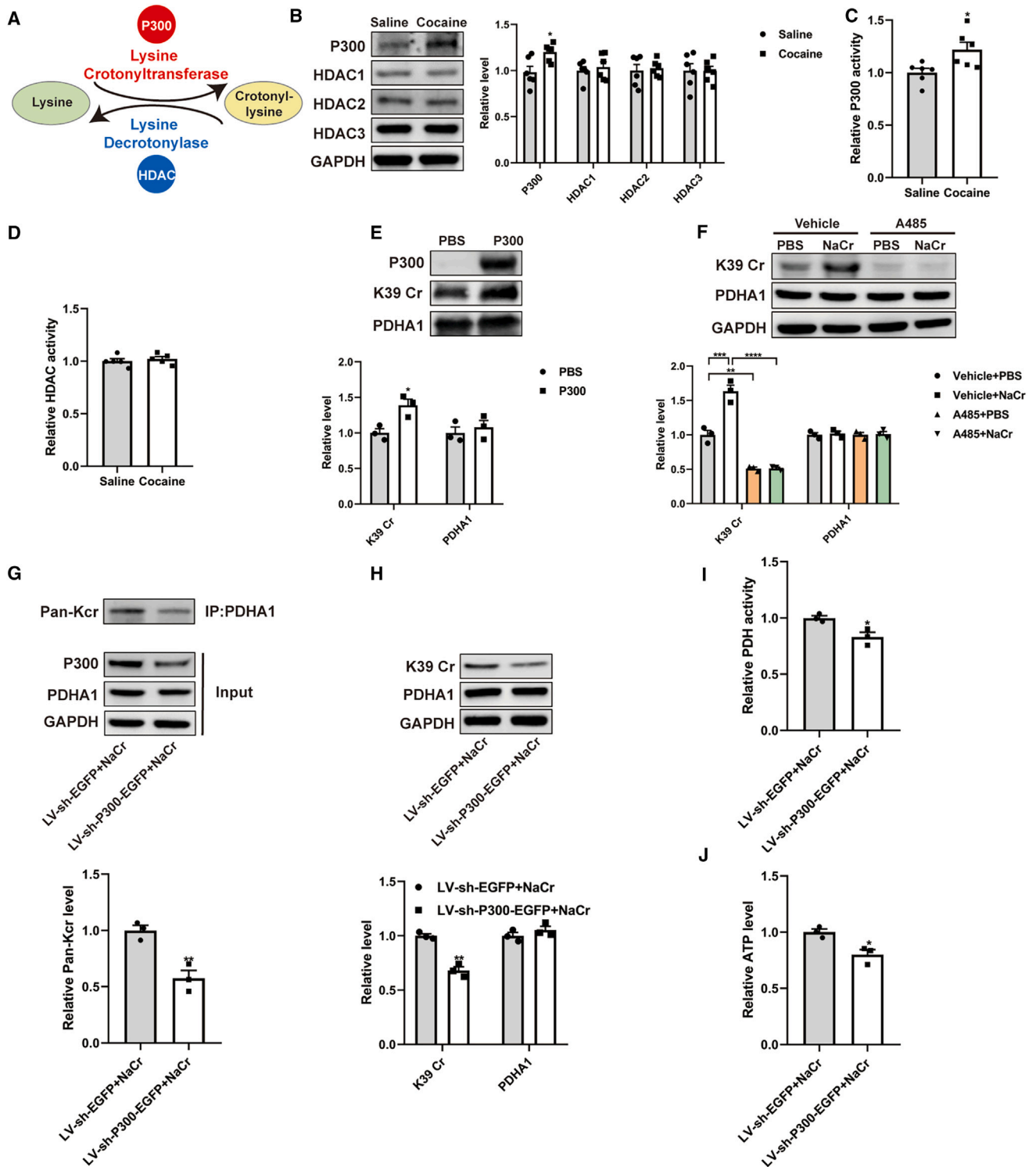


Figure 4. PDHA1 K39 is crotonylated by P300

(A) Schematic of the regulatory enzymes of protein Kcr.

(B) Western blotting analysis showing the levels of P300 and HDAC1-3 in the dDG after CPP training ($n = 6$ per group).

(C and D) P300 activity was increased, but HDAC activity was not altered, in the dDG after CPP training (P300 activity: $n = 6$ per group; HDAC activity: $n = 5$ per group).

(E) Western blotting analysis showing the level of K39 Cr in recombinant PDHA1 after P300 treatment.

(legend continued on next page)

acylating enzymes (Figure 3D), indicating the direct effect of NaCr on PDHA1 K39 Cr.

Finally, we explored the role of PDHA1 K39 Cr in dDG neurons in cocaine-associated memory. To this end, we stereotaxically injected AAV-CaMKII-PDHA1 or AAV-CaMKII-mutant PDHA1 into the dDG of conditional KO (cKO) mice (CaMKII-*creERT2*^{+/-}; PDHA1^{fl/fl} mice) 3 weeks before CPP training. The mice were then intraperitoneally injected with tamoxifen to deplete endogenous PDHA1 in excitatory neurons 2 weeks before cocaine CPP training (Figures S6A–S6C; PDHA1 relative level $t_{(10)} = 9.944$, $p < 0.0001$; PDHA1 relative fluorescence intensity $t_{(4)} = 7.001$, $p < 0.01$). NaCr was microinfused into the dDG of mice through an implanted cannula 30 min before CPP training (Figure 3E). After low-dose (2.5 mg/kg) cocaine CPP training, the CPP score were not significantly increased (Figures S7A and S7B), suggesting that low-dose cocaine failed to induce cocaine-associated memory formation. However, compared with exogenous mutant PDHA1-overexpressing mice, mice with exogenous PDHA1 overexpression in hippocampal neurons displayed a significant increase in the CPP score after low-dose cocaine (2.5 mg/kg) CPP training (Figures 3F and 3G; CPP score treatment: $F_{(1, 40)} = 54.85$, $p < 0.0001$; time: $F_{(3, 40)} = 4.176$, $p < 0.05$; interaction: $F_{(3, 40)} = 4.198$, $p < 0.05$). These results indicated that PDHA1 K39 Cr in hippocampal neurons contributed to cocaine-associated memory recall.

P300 catalyzes PDHA1 K39 Cr in hippocampal neurons

Because Kcr is dynamically regulated by the opposing enzymatic activity of lysine crotonyltransferase and lysine decrotonylase (Figure 4A),^{13,17} we sought to identify the kinase responsible for PDHA1 K39 Cr. The levels of hippocampal P300 (lysine crotonyltransferase) and HDAC1–3 (lysine decrotonylase) in the dDG were analyzed after cocaine CPP training. We found that both the level and activity of P300 increased in the dDG, whereas the levels of HDAC1, -2, and -3 and total HDAC activity did not change (Figures 4B–4D; P300 $t_{(10)} = 2.936$, $p < 0.05$; P300 activity $t_{(10)} = 2.695$, $p < 0.05$). Furthermore, incubation of recombinant PDHA1 and P300 with crotonoyl-CoA at 37°C for 3 h significantly increased the level of PDHA1 K39 Cr (Figure 4E; $t_{(4)} = 3.714$, $p < 0.05$), indicating that P300 may act as a lysine crotonyltransferase to regulate PDHA1 K39 Cr. To determine whether P300 is responsible for PDHA1 K39 Cr, we treated HT22 cells with a P300 inhibitor (A485, 3 μ M) or knocked down P300 in HT22 cells using P300 shRNA. Results showed that NaCr (20 mM) markedly increased the level of K39 Cr, whereas A485 treatment decreased the level of K39 Cr in the cells regardless of NaCr pretreatment (Figure 4F; K39 Cr $F_{(3, 8)} = 119.4$, $p < 0.0001$). In addition, P300 deficiency decreased the levels of PDHA1 Pan-Kcr and K39 Cr in HT22 cells after NaCr treatment (Figures 4G and 4H; Pan-PDHA1 Kcr $t_{(4)} = 5.056$, $p < 0.01$; K39 Cr $t_{(4)} = 8.359$, $p < 0.01$). As expected, PDH activity and ATP levels were significantly reduced in P300-deficient cells compared with control

cells after NaCr treatment (Figures 4I and 4J; PDH activity, $t_{(4)} = 3.586$, $p < 0.05$; ATP activity, $t_{(4)} = 3.793$, $p < 0.05$). These results indicated that P300 is responsible for PDHA1 K39 Cr, the inhibition of which can suppress PDH activity and energy production.

PDHA1 K39 Cr promotes PDH activity and pyruvate metabolism in hippocampal neurons

To better understand the effect of PDHA1 K39 Cr on PDH activity, overexpression of PDHA1 shRNA-resistant exogenous PDHA1 or mutant PDHA1 was induced in endogenous PDHA1-depleted HT22 cells (Figure 5A). NaCr treatment (20 mM) increased PDH activity in the cells overexpressing PDHA1; nevertheless, these effects were reversed by the overexpression of mutant PDHA1 in the cells (Figure 5B; $F_{(3, 12)} = 5.548$, $p < 0.05$). Similarly, the acetyl-CoA and ATP levels were increased but the ADP level was decreased in the PDHA1-overexpressing cells. However, the opposite effects were observed in mutant PDHA1-overexpressing cells (Figures 5C–5E; acetyl-CoA $F_{(3, 12)} = 4.72$, $p < 0.05$; ATP $F_{(3, 12)} = 5.240$, $p < 0.05$; ADP $F_{(3, 12)} = 4.759$, $p < 0.05$). As PDH activity is inhibited by the phosphorylation of PDHA1, we further tested whether PDHA1 K39 Cr could regulate PDH activity by affecting PDHA1 phosphorylation. We found that NaCr treatment failed to change the level of PDHA1 phosphorylated at serine 293 in endogenous PDHA1-depleted HT22 cells overexpressing PDHA1 or mutant PDHA1 (Figure S8A).

Considering that the PDHA1 PTM plays an important role in regulating pyruvate metabolism in mitochondria,²³ we investigated whether PDHA1 K39 Cr could alter mitochondrial function. The oxygen consumption rate (OCR) of HT22 cells overexpressing PDHA1 or mutant PDHA1 was measured using a Seahorse XF 24 extracellular flux analyzer. We found that the OCR was significantly increased in PDHA1-overexpressing cells after treatment with NaCr (20 mM) for 24 h, indicating enhanced mitochondrial respiration/oxygen consumption (Figure 5F). Furthermore, ATP production, maximal respiration, and spare respiratory capacity were increased in PDHA1-overexpressing cells but not in mutant PDHA1-overexpressing cells (Figures 5G–5K; ATP production $F_{(2, 10)} = 9.273$, $p = 0.0053$; maximal respiration $F_{(2, 10)} = 7.137$, $p < 0.05$; spare respiratory capacity $F_{(2, 10)} = 9.638$, $p < 0.05$).

Finally, to evaluate whether PDHA1 K39 Cr regulates the TCA cycle by directly facilitating pyruvate metabolism, we performed ¹³C-labeled pyruvate tracing experiments. After NaCr treatment for 24 h, the levels of ¹³C-labeled pyruvate incorporation in TCA cycle metabolites increased in the HT22 cells overexpressing PDHA1; however, a similar increase was not observed in the cells overexpressing mutant PDHA1 (Figure 5L). Collectively, our data showed that PDHA1 K39 Cr is a critical PTM for PDH activation, which is necessary for promoting pyruvate metabolism and the TCA cycle.

(F) Western blotting analysis showing the levels of K39 Cr and PDHA1 in HT22 cells after A485 treatment ($n = 3$ per group).

(G) Western blotting analysis showing the level of Pan-Kcr in P300-deficient HT22 cells after NaCr treatment ($n = 3$ per group).

(H) Western blotting analysis showing the levels of K39 Cr and PDHA1 in P300-deficient HT22 cells after NaCr treatment ($n = 3$ per group).

(I and J) PDH activity and ATP levels were decreased in P300-deficient HT22 cells after NaCr treatment ($n = 3$ per group).

The data are the means \pm SEMs. Unpaired t test or one-way ANOVA, * $p < 0.05$, ** $p < 0.01$, *** $p < 0.001$, and **** $p < 0.0001$.

PDHA1 K39 Cr regulates neuronal activity and energy production during cocaine-associated memory formation

Because PDH activation-mediated neuronal ATP production is essential for neuronal activity,⁴ we investigated whether PDHA1 K39 Cr and ATP production are essential for hippocampal neuronal activity during cocaine-associated memory formation. To stimulate neuronal activity *in vitro*, HT22 cells were treated with KCl (40 mM) for 1 h.^{4,33} We found that the level of c-Fos, a marker of neuronal activation, was significantly increased, which was accompanied by increased levels of both PDHA1 K39 Cr and ATP; nevertheless, the total PDHA1 expression level did not change (Figures 6A and 6B; c-Fos $t_{(4)} = 3.535$, $p < 0.05$; K39 Cr $t_{(4)} = 4.213$, $p < 0.05$; ATP $t_{(6)} = 3.295$, $p < 0.05$). These results suggested that neuronal activation was indeed associated with PDHA1 K39 Cr and ATP production. Next, to validate whether neuronal activity depends on ATP production driven by PDHA1 K39 Cr, endogenous PDHA1-depleted HT22 cells overexpressing PDHA1 or mutant PDHA1 were pretreated with NaCr (20 mM) for 24 h and then activated with KCl (40 mM) for 1 h. We found significantly increased expression of c-Fos in the cells overexpressing PDHA1 (Figure 6C; $F_{(3,8)} = 24.28$, $p < 0.001$). Immunostaining analysis also showed that the cells overexpressing PDHA1 exhibited strong c-Fos fluorescence after KCl treatment (Figures 6D and 6E; $F_{(3,8)} = 56.97$, $p < 0.0001$). Consistently, ATP production was significantly greater in PDHA1-overexpressing cells than in control cells (Figure 6F; $F_{(3,12)} = 20.12$, $p < 0.0001$). Finally, we examined the role of PDHA1 K39 Cr in neuronal activation in the presence of brain-derived neurotrophic factor (BDNF), a physiological stimulator of neuronal activation. BDNF (50 ng/mL) treatment increased the level of c-Fos in HT22 cells overexpressing PDHA1 (Figure 6G; $F_{(3,8)} = 13.27$, $p < 0.01$). In the endogenous PDHA1-depleted HT22 cells, overexpressing mutant PDHA1 failed to increase the c-Fos level or ATP production after KCl (40 mM) treatment for 1 h (Figures S9A and S9B; $F_{(3,12)} = 7.818$, $p < 0.01$). Together, these results indicated that PDHA1 K39 Cr functions as a critical PTM necessary for hippocampal neuronal activation.

PDHA1 K39 Cr regulates neuronal activity and energy production during cocaine-associated memory formation

To further determine whether PDHA1 K39 Cr regulates cocaine memory formation by promoting hippocampal dDG neuronal activity, we manipulated dDG neuronal activity *in vivo* using a

chemogenetic approach with a designer receptor exclusively activated by designer drugs. To induce dDG neuron activation, we induced selective expression of hM3D (Gq) in dDG neurons. The dDGs of the mice were bilaterally injected with a virus expressing hM3D (Gq) under the CaMKII promoter (AAV-CaMKII-hM3D (Gq)) and then subjected to low-dose cocaine (2.5 mg/kg) CPP training (Figure S10A). Thirty minutes before the CPP test, all the mice were injected with clozapine-N-oxide (CNO, 0.2 mg/kg) to activate dDG neurons. Notably, the CPP score of the mice with activated dDG neurons was significantly greater than that of the control mice (Figure S10B; treatment $F_{(1,56)} = 26.57$, $p < 0.0001$; time $F_{(3,56)} = 4.866$, $p < 0.05$; interaction $F_{(3,56)} = 5.150$, $p < 0.05$). Western blotting analysis revealed significantly increased c-Fos levels in the dDG of mice injected with AAV-CaMKII-hM3D (Gq) after the cocaine CPP test (Figure S10C, $F_{(3,20)} = 18.96$, $p < 0.0001$). In contrast, to suppress dDG neuron activity, the dDGs of the mice were bilaterally injected with a virus expressing hM4D (Gi) under the CaMKII promoter (AAV-CaMKII-hM4D (Gi)), and the mice were then subjected to cocaine CPP training. Thirty minutes before the cocaine CPP test, the mice were injected with CNO (5 mg/kg) to suppress dDG neuron activity (Figure S10D). Importantly, inhibition of dDG neuronal activity significantly inhibited cocaine-associated memory recall, as evidenced by a significant decrease in the CPP score (Figure S10E; treatment $F_{(1,56)} = 26.55$, $p < 0.0001$; time $F_{(3,56)} = 9.024$, $p < 0.0001$; interaction $F_{(3,56)} = 8.914$, $p < 0.0001$). Western blotting analysis showed that c-Fos expression in the dDG was almost abolished when neuronal activity was suppressed by CNO (Figure S10F, $F_{(3,20)} = 266.7$, $p < 0.0001$). In addition, to confirm whether manipulating dDG neuronal activity during conditioning affects cocaine-associated memory formation, we activated or inhibited dDG neuron activity during conditioning (Figures S10G and S10I). Behavioral analyses revealed that excitation or inhibition of dDG neuron activity had no effect on cocaine-associated memory despite the CPP score changing after dDG neuron activity was manipulated during conditioning (Figures S10H and S10J; treatment $F_{(1,14)} = 16.35$, $p < 0.01$; time $F_{(3,42)} = 11.2$, $p < 0.0001$; interaction $F_{(3,42)} = 11.12$, $p < 0.001$). Together, these results indicate that neuronal activity in the dDG is necessary for cocaine-associated memory recall.

We continued to explore whether PDHA1 K39 Cr affects cocaine-associated memory by regulating hippocampal neuron activity in the dDG. A PDHA1- or mutant PDHA1-expressing AAV (AAV-CaMKII-PDHA1 or AAV-CaMKII-mutant PDHA1) was infused into the dDG of cKO mice (CaMKII-*creERT2*^{+/-};

Figure 5. K39 Cr of PDHA1 regulates mitochondrial pyruvate metabolism by increasing PDH activity

(A) Western blotting analysis showing the level of FLAG in PDHA1-deficient HT22 cells overexpressing exogenous PDHA1 or mutant PDHA1 after NaCr treatment ($n = 5$ per group).

(B–E) The levels of PDH activity, acetyl-CoA, ATP, and ADP were measured in PDHA1-deficient HT22 cells overexpressing exogenous WT or mutant PDHA1 after NaCr treatment ($n = 4$ per group).

(F–K) The real-time oxygen consumption rate (OCR), base respiration, ATP levels, H⁺ proton leakage, maximal respiration, and spare respiratory capacity were analyzed in PDHA1-deficient HT22 cells overexpressing exogenous WT or mutant PDHA1 after NaCr treatment ($n = 5$ for the PBS+LV-PDHA1 group; $n = 4$ for the NaCr+LV-PDHA1 group; $n = 4$ for the NaCr+LV-mutant-PDHA1 group).

(L) The enrichment of isotopes derived from ¹³C₃-labeled pyruvate in TCA intermediates was determined by mass spectrometry analysis ($n = 3$ per group). Red circle: ¹³C-labeled carbon atom derived from ¹³C₃-labeled pyruvate; white circle: unlabeled carbon atom. M+2: two ¹³C-labeled carbon atoms derived from ¹³C₃-labeled pyruvate.

The data are the means ± SEMs. One-way ANOVA, * $p < 0.05$, ** $p < 0.01$, and *** $p < 0.001$.

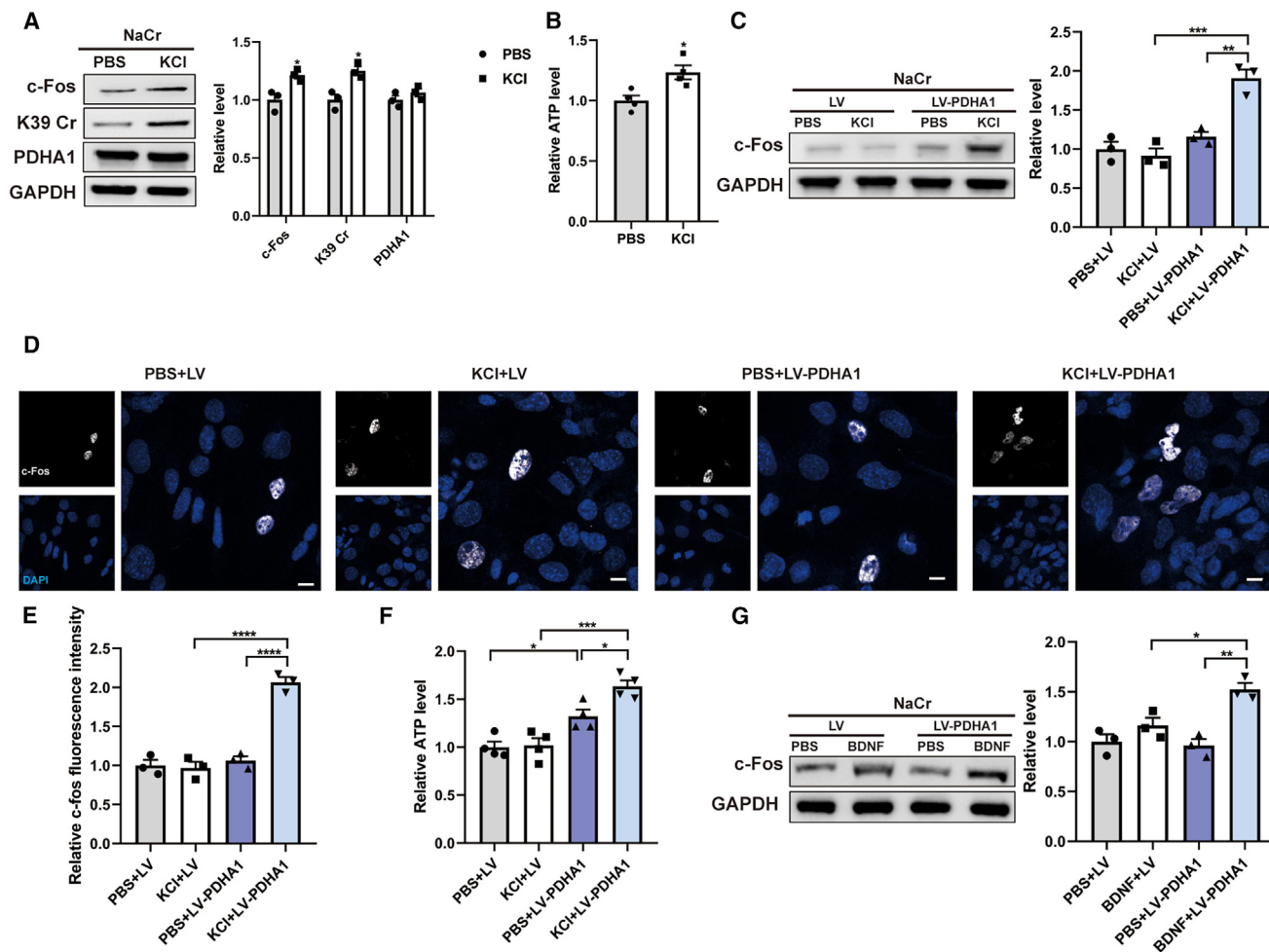


Figure 6. K39 Cr of PDHA1 regulates neuron activation by promoting energy production

(A) Western blotting analysis showing the levels of c-Fos, K39 Cr, and PDHA1 in HT22 cells pretreated with NaCr after KCl stimulation ($n = 3$ per group).

(B) ATP levels were decreased in HT22 cells pretreated with NaCr after KCl stimulation ($n = 4$ per group).

(C) Western blotting analysis showing the level of c-Fos in endogenous PDHA1-deficient HT22 cells and PDHA1-deficient HT22 cells overexpressing exogenous PDHA1 (pretreated with NaCr) after KCl stimulation ($n = 3$ per group).

(D and E) Immunostaining analysis showing the c-Fos fluorescence intensity in endogenous PDHA1-deficient HT22 cells and PDHA1-deficient cells overexpressing exogenous PDHA1 (pretreatment with NaCr) after KCl stimulation. Scale bar, 10 μ m

(F) The level of ATP was increased in PDHA1-deficient cells overexpressing exogenous PDHA1 (pretreated with NaCr) after KCl stimulation ($n = 4$ per group).

(G) Western blotting analysis showing the level of c-Fos in endogenous PDHA1-deficient HT22 cells and PDHA1-deficient cells overexpressing exogenous PDHA1 (pretreated with NaCr) after BDNF stimulation ($n = 3$ per group).

The data are the means \pm SEMs. Unpaired t test or one-way ANOVA, * $p < 0.05$, ** $p < 0.01$, *** $p < 0.001$, and **** $p < 0.0001$.

PDHA1^{fl/fl} mice) 3 weeks before CPP training. The mice were intraperitoneally injected with tamoxifen to deplete endogenous PDHA1 in excitatory neurons 2 weeks before CPP training (Figure 7A). We observed that mice with PDHA1 knockdown in excitatory neurons showed a lower CPP score than wild-type mice; however, the mice with exogenous PDHA1 overexpression in the dDG showed a significant increase in the CPP score, while mice overexpressing mutant PDHA1 failed to show this change (Figure 7B; treatment $F_{(1,64)} = 46.15$, $p < 0.0001$; time $F_{(3,64)} = 3.096$, $p < 0.05$; interaction $F_{(3,64)} = 3.4$, $p < 0.05$). Moreover, the decreases in the levels of c-Fos and ATP in cKO mice were reversed after overexpressing PDHA1, but not mutant PDHA1,

in the dDG (Figures 7C and 7D; c-Fos $F_{(3,20)} = 14.96$, $p < 0.001$; ATP $F_{(3,12)} = 15.68$, $p < 0.001$). Immunostaining analysis further verified that overexpression of PDHA1 reversed the decrease in the level of c-Fos in the dDG of cKO mice subjected to cocaine conditions (Figure 7E; $F_{(3,8)} = 12.13$, $p < 0.01$). Finally, we explored whether PDHA1 K39 Cr affects the expression of activity-regulated cytoskeletal-associated protein (Arc), another immediate-early gene, during cocaine-associated memory formation. Western blotting revealed that the expression of Arc was also decreased in the dDGs of cKO mice, and this decrease was reversed after overexpressing PDHA1 (Figure S11A; $F_{(3,20)} = 11.02$, $p < 0.001$). Collectively, our results demonstrated that

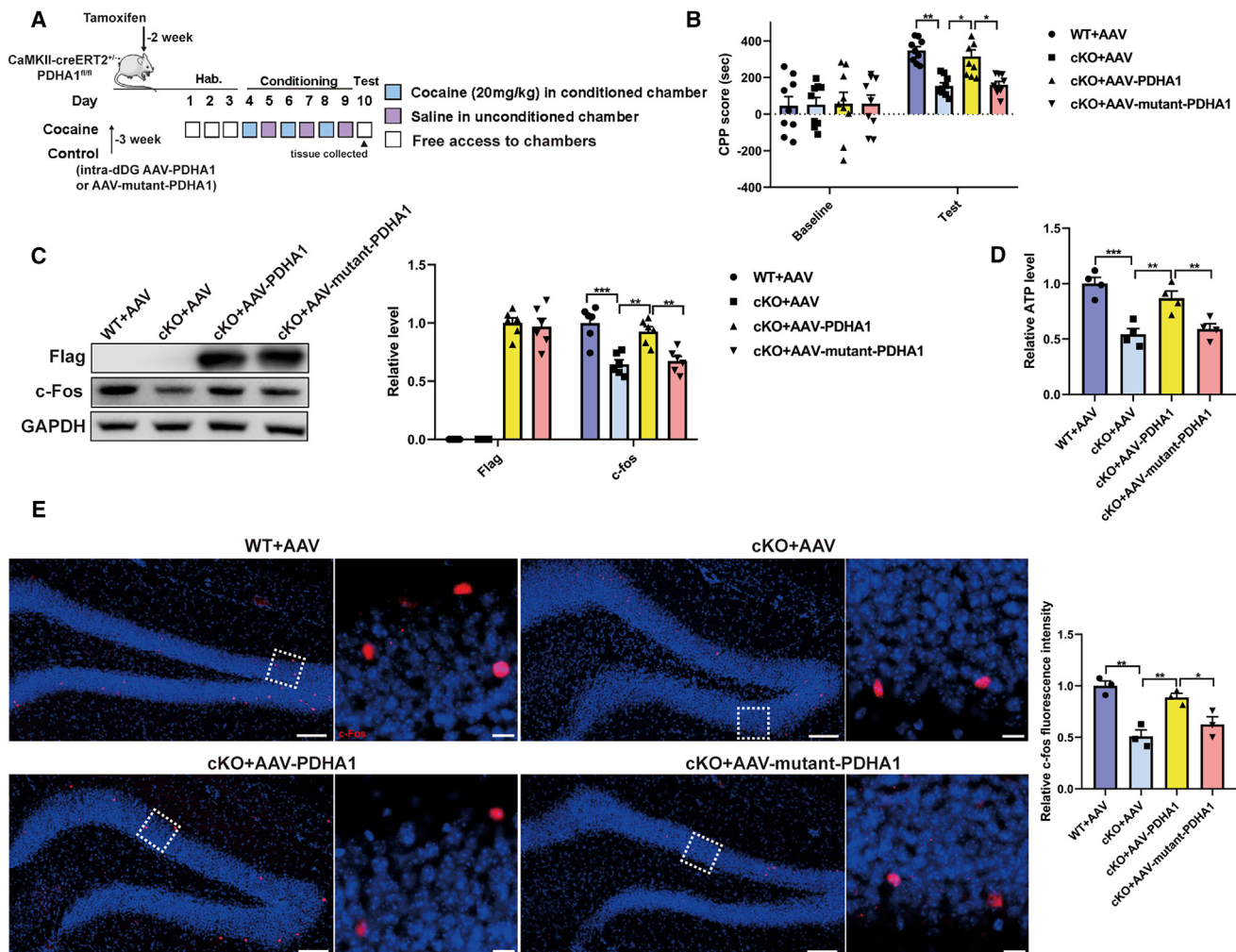


Figure 7. K39 Cr of PDHA1 mediates cocaine-associated memory formation through activation of dDG neurons

(A) Schematic diagram of the experimental design for AAV and tamoxifen injection, brain stereotaxic surgery, NaCr administration, and cocaine CPP training.

(B) AAV-mediated PDHA1 overexpression in the dDG reversed the decrease in the cocaine CPP score in cKO mice ($n = 9$ per group).

(C) Western blotting analysis showing the levels of FLAG and c-Fos in the dDG of mice after CPP training ($n = 6$ per group).

(D) The level of ATP was increased in the dDG of mice with PDHA1 overexpression after CPP training ($n = 4$ per group).

(E) Immunostaining analysis showing the c-Fos fluorescence intensity in the dDG of mice after CPP training ($n = 3$ per group). Long scale bar, 100 μm . Short scale bar, 10 μm .

The data are the means \pm SEMs. One-way or two-way ANOVA, * $p < 0.05$, ** $p < 0.01$, and *** $p < 0.001$. Hab, habituation.

PDHA1 K39 Cr mediates cocaine-associated memory recall by promoting dDG neuronal activity in an ATP production-dependent manner.

DISCUSSION

Neuronal activity requires a mechanism in which local energy consumption can be spatially matched to energy generation in response to extracellular stimuli.⁵ Neurons can adapt to utilize glycolysis, oxidative phosphorylation, and fatty acid β -oxidation to meet energy demands during drug exposure.^{27,34–36} In the present study, we characterized the functional significance of PDHA1 K39 Cr in the dDG of mice conditioned by cocaine

CPP. Our results showed that PDHA1 K39 Cr promoted pyruvate metabolism and ATP production to trigger neuronal activation in the dDG and provide insight into how Kcr of a key TCA metabolic enzyme regulates cocaine-associated memory. These findings reveal a link between neuroenergetics and drug addiction from the perspective of hippocampal neuron activation.

Studies have shown that neuronal energy production is dynamically regulated in multiple ways and necessary for the maintenance of neuronal activity in response to different stimuli.^{4,37} For example, Rheb acts as a hub protein that regulates neuronal activity and neuroenergetics via Rheb-PDH axis-mediated pyruvate metabolism.⁴ AMPK may be responsible for neuronal-activity-induced energy production by increasing the

localization of glucose transporter 4 to presynaptic terminals and glycolysis.³⁸ Glia-derived lactate, an energy substrate for neurons, is converted to pyruvate for ATP production through oxidative phosphorylation in mitochondria.³⁹ In addition, lactate-fueled neuroenergetics may be essential for sustaining neuronal function during periods of heightened activity.⁴⁰ In this study, PDHA1 Kcr-mediated PDH activation was shown to be an important mechanism by which neurons drive pyruvate metabolism and ATP production to become activated. We infer that hippocampal neurons can undergo metabolic enhancement via mitochondrial oxidative phosphorylation to cope with cocaine stress conditions. A consequence of this metabolic enhancement is that neurons become able to produce more ATP rapidly, thus facilitating cocaine memory processing. Together with previous studies, these findings further support the notion that neuronal energy consumption is increased when neurons are in an activated state.⁴¹

As neurons lack energy stores, multiple cellular and molecular mechanisms, including the regulation of key TCA metabolic enzymes, may contribute to enhancing energy production and maintaining ATP homeostasis.⁴² Studies have shown that the learning process results in lactate release in the hippocampus and that the transfer of lactate from astrocytes to neurons is essential for long-term memory formation.⁴³ Disruption of lactate transfer in the basolateral amygdala impairs cocaine-associated memory, supporting a role for lactate in mediating intracellular responses for drug memory.^{34,35} Our results reveal a mechanism by which cocaine-associated memory forms through neuronal pyruvate metabolism and energy production. In fact, studies have shown the important role of PDHA1 in learning and memory.⁴⁴ PDHA1 KO increases the extracellular acidification rate and lactate levels but decreases ATP production in hippocampal neurons, indicating that PDHA1-deleted neurons cannot perform normal mitochondrial oxidative phosphorylation to provide sufficient energy for neuronal function.⁴⁵ In addition, PDHA1 KO in the hippocampus leads to the accumulation of lactate and impairs gene-expression-associated learning and memory.⁴⁵ Similarly, we observed that PDHA1 KO decreased PDH activity, pyruvate metabolism, and ATP production in hippocampal neurons, thus reducing the formation of cocaine-associated memory in mice. These findings suggest that due to the loss of PDHA1, neurons cannot sufficiently utilize energy substrates; therefore, weakened energy production cannot support heightened neuronal function adaptable to the rewarding effect of cocaine. Similarly, dysregulated pyruvate accumulation impairs memory and cognitive function, which results from weakened PDH activity and ATP synthesis.⁴⁶ These studies are in line with our findings, supporting the notion that neuroenergetics through PDHA1 regulation play an important role in maintaining heightened neuronal function and that dysregulated energy metabolism in hippocampal neurons can disrupt memory formation.

We identified 14,072 Kcr sites in 3,128 proteins of the dDG after the cocaine CPP paradigm, which expands the crotonylome and provides a more comprehensive cellular Kcr landscape than that observed in previous studies of global Kcr profiles.^{16,47} Among the proteins that undergo cocaine-induced Kcr, PDHA1 was identified to be crotonylated at the K39 residue, which is crit-

ical for activating PDH and promoting pyruvate metabolism. In contrast, when PDHA1 K39 in the hippocampus was mutated, neither cocaine nor NaCr treatment affected PDHA1 function *in vivo* or *in vitro*. These results indicate that PDHA1 K39 Cr can directly modulate PDH activity, further supporting the currently accepted mechanisms of PDH activity regulation through PDHA1 PTMs.⁴⁸

Previous studies have shown that PDHA1 activity can be regulated by various PTMs, including phosphorylation and acetylation. For example, phosphorylation of PDHA1 at S295 and S314 by AMPK is essential for the maintenance of PDH activity and TCA cycle regulation in breast cancer cells.²³ PDHA1 acetylation at K321 results in the recruitment of PDK1 to inhibit PDHA1 S293 phosphorylation and PDH activity in lung cancer cells.²⁴ Our findings reveal a link between PDHA1 Kcr and the regulation of pyruvate metabolism in hippocampal neurons during cocaine-associated memory formation.

Studies have shown that P300 regulates histone Kcr and directly stimulates transcription to a greater degree than histone acetylation.³¹ Interestingly, we found that P300 was upregulated by cocaine and catalyzed Kcr on nonhistone proteins. Treatment with the P300 selective inhibitor A485 or knockdown of P300 by shRNA resulted in a drastic reduction in PDHA1 K39 Cr in HT22 cells, indicating that P300 acts as a major upstream crotonyltransferase for PDHA1 Kcr. P300 appears to prefer the substrate NaCr for Kcr but not for lysine acylation, as evidenced by the Cr of PDHA1 K39 in NaCr-treated cells. We speculate that there is an internal regulatory mechanism by which P300 selects substrates for either Kcr or lysine acylation under different stress conditions. In addition to P300, the writer of PDHA1 Kcr, it will be interesting to investigate the eraser protein, which may uncover the multilayered regulatory topology of PDHA1 Kcr in neurons in response to psychostimulants.

The dorsal hippocampus is the key brain region for the formation of drug reward memory.^{49,50} Cocaine-addicted individuals show profound neurobiological alterations in the hippocampus, as evidenced by dysregulation of hippocampal neuron functional activity and connectivity.⁵¹ Artificially increasing the activity of a similar small population of neurons thought to be in a memory trace impacts cocaine-associated memory formation.^{52,53} Before cue-cocaine pairing training, CREB overexpression or excitatory optogenetic activation of a random sparse population of neurons in the lateral amygdala is sufficient to enhance cocaine-associated memory.^{52,53} Together with our findings, these results support the notion that activated neurons are preferentially allocated to support cocaine-associated memory formation. In the present study, chemogenetically promoting or inhibiting the excitability of dDG neurons enhanced or weakened cocaine reward memory, respectively, indicating that regulated neurons in the dDG affect reward memory formation. Similarly, optogenetic activation of a small number of dDG neurons during context fear training induces freezing behavior,⁵⁴ suggesting that activation of these cells serves as a sufficient retrieval cue for the expression of fear memory. Because a difference in fear and reward memory is the type of training that occurs and can be considered an aversive or rewarding experience, we consider that dDG neurons may not specifically sort aversive or rewarding memories. In addition, memory-coding neurons are thought to

be especially sparse in the dDG,⁵⁵ which may help explain why a small number of dDG neurons are activated during cocaine CPP training.

In conclusion, cocaine enhanced PDHA1 K39 Cr in hippocampal neurons, thus promoting pyruvate metabolism and ATP production, which are necessary for cocaine-associated memory recall. The reprogramming of neuronal pyruvate metabolism could be a promising strategy for maintaining or restoring the physiological functions of neurons and thus potentially alleviating cocaine-associated memory.

Limitations of the study

In this study, we made great efforts to analyze the role of protein Kcr in cocaine-associated memory and found that differentially Kcr proteins were most significantly enriched in energy metabolism pathways. We validated the Kcr of enzymes involved in energy metabolism and further proved that the Cr of PDHA1 at the K39 site promotes pyruvate metabolism to increase neuronal activity for cocaine-associated memory recall. However, we cannot rule out the possibility that PDHA1 undergoes other PTMs, including acetylation, during cocaine-associated memory formation. In addition, other types of PTMs may participate in crosstalk with the Cr of PDHA1, but how PDH activity and pyruvate metabolism are coregulated remains unknown. Furthermore, we demonstrated that the activity of PDH is regulated by PDHA1 K39 Cr. Researchers will need to assess precisely how PDH is regulated by PDHA1 K39 Cr by co-immunoprecipitation or molecular dynamics simulations in the future. Finally, in addition to P300, the writer of PDHA1 Kcr, it will be interesting to investigate eraser proteins, which will deepen our understanding of how Kcr affects PDHA1 function in hippocampal neurons in response to psychostimulants.

STAR★METHODS

Detailed methods are provided in the online version of this paper and include the following:

- KEY RESOURCES TABLE
- RESOURCES AVAILABILITY
 - Lead contact
 - Materials availability
 - Data and code availability
- EXPERIMENTAL MODEL AND STUDY PARTICIPANT DETAILS
 - Animals
 - Cell lines
 - Drugs
- METHOD DETAILS
 - Clozapine-N-oxide (CNO) administration
 - Behavioral paradigm
 - CPP
 - Pretest session
 - CPP training
 - CPP test
 - Food CPP
 - Home cage cocaine injection
 - Locomotor activity
 - Contextual fear conditioning
 - Stereotactic surgery and drug administration
 - Stereotactic surgery and adeno-associated virus injection
 - Lentiviral vector construction and cell transfection
 - Tissue isolation

- Western blot
- Co-immunoprecipitation
- Western blotting analysis of PDHA1, β -adducin and PFKM lysine crotonylation
- Enzymatic assay of PDH activity
- Pyruvate metabolite assays
- Seahorse assay
- ¹³C-labeled pyruvate tracing
- Immunohistochemistry
- Immunocytochemistry
- PDHA1 crotonylation *in vitro*
- P300-catalyzed PDHA1 crotonylation *in vitro*
- Protein purification
- Dot blots
- LC-MS/MS analysis of protein crotonylation
- HPLC fractionation
- Kcr peptide enrichment
- LC-MS/MS analysis
- Database searching and protein quantification
- Bioinformatics analysis
- QUANTIFICATION AND STATISTICAL ANALYSIS

SUPPLEMENTAL INFORMATION

Supplemental information can be found online at <https://doi.org/10.1016/j.celrep.2024.114529>.

ACKNOWLEDGMENTS

We are grateful to PTM Biolabs Co., Ltd., for the Kcr proteomics analysis and Yuanhong Deng, Shuang Zheng, and their colleagues (PTM Biolabs Co., Ltd., Hangzhou, China) for the MS analysis of PDHA1 Kcr. We also thank Maodi Xie (Laboratory of Mitochondria and Metabolism, West China Hospital, Sichuan University) for providing the corresponding Seahorse assay instruments and experimental methods. This work was partially supported by the National Natural Science Foundation of China (grants 82071494 and 82371498); the 1·3·5 Project for Disciplines of Excellence, West China Hospital, Sichuan University (ZYG23011); the Postdoctoral Research Fund of West China Hospital of Sichuan University (2021HXBH007); the a project funded by the China Postdoctoral Science Foundation (2021M702373); the Postdoctoral Research Fund of Sichuan University (2023SCU12058); and the National Natural Science Foundation of Sichuan Province (2022NSFSC1580).

AUTHOR CONTRIBUTIONS

Conceived and designed the experiments, interpreted the data, provided financial support, and wrote the manuscript, H.L.; performed the experiments, acquired the data, and analyzed and interpreted the data, X.L.; methodology, R.C., L.B., J.Z., Yue Zhao, Y.X., L.W., F.Q., Y.C., S.H., Q.W., S.L., and D.Z.; data acquisition and statistical analysis, X.L., W.X., Y. Zhou, N.Z., and Q.B.; interpretation of the findings and revision of the manuscript, Ying Zhao, X.W., L.J., Y.D., N.Z., W.K., M.Q., H.W., J.T., and Yinglan Zhao; conceived and supervised the research, provided financial support, and revised the manuscript, X.C.

DECLARATION OF INTERESTS

The authors declare no competing interests.

Received: January 8, 2024

Revised: June 4, 2024

Accepted: July 8, 2024

REFERENCES

- Zhou, Y., Zhu, H., Liu, Z., Chen, X., Su, X., Ma, C., Tian, Z., Huang, B., Yan, E., Liu, X., and Ma, L. (2019). A ventral CA1 to nucleus accumbens core engram circuit mediates conditioned place preference for cocaine. *Nat. Neurosci.* 22, 1986–1999. <https://doi.org/10.1038/s41593-019-0524-y>.
- Li, H., Xu, W., Wang, D., Wang, L., Fang, Q., Wan, X., Zhang, J., Hu, Y., Li, H., Zhang, J., et al. (2021). 4R Tau Modulates Cocaine-Associated Memory through Adult Dorsal Hippocampal Neurogenesis. *J. Neurosci.* 41, 6753–6774. <https://doi.org/10.1523/JNEUROSCI.2848-20.2021>.
- Bender, B.N., and Torregrossa, M.M. (2020). Molecular and circuit mechanisms regulating cocaine memory. *Cell. Mol. Life Sci.* 77, 3745–3768. <https://doi.org/10.1007/s00018-020-03498-8>.
- Yang, W., Pang, D., Chen, M., Du, C., Jia, L., Wang, L., He, Y., Jiang, W., Luo, L., Yu, Z., et al. (2021). Rheb mediates neuronal-activity-induced mitochondrial energetics through mTORC1-independent PDH activation. *Dev. Cell* 56, 811–825.e6. <https://doi.org/10.1016/j.devcel.2021.02.022>.
- Rangaraju, V., Calloway, N., and Ryan, T.A. (2014). Activity-driven local ATP synthesis is required for synaptic function. *Cell* 156, 825–835. <https://doi.org/10.1016/j.cell.2013.12.042>.
- Miguens, M., Kastanauskaitė, A., Coria, S.M., Selvas, A., Ballesteros-Yanez, I., DeFelipe, J., and Ambrosio, E. (2015). The effects of cocaine self-administration on dendritic spine density in the rat hippocampus are dependent on genetic background. *Cereb Cortex* 25, 56–65. <https://doi.org/10.1093/cercor/bht200>.
- Gabach, L.A., Carlini, V.P., Monti, M.C., Maglio, L.E., De Barioglio, S.R., and Perez, M.F. (2013). Involvement of nNOS/NO/sGC/cGMP signaling pathway in cocaine sensitization and in the associated hippocampal alterations: does phosphodiesterase 5 inhibition help to drug vulnerability? *Psychopharmacology (Berl)* 229, 41–50. <https://doi.org/10.1007/s00213-013-3084-y>.
- Blanco, E., Bilbao, A., Luque-Rojas, M.J., Palomino, A., Bermudez-Silva, F.J., Suarez, J., Santin, L.J., Estivill-Torres, G., Gutierrez, A., Campos-Sandoval, J.A., et al. (2012). Attenuation of cocaine-induced conditioned locomotion is associated with altered expression of hippocampal glutamate receptors in mice lacking LPA1 receptors. *Psychopharmacology (Berl)* 220, 27–42. <https://doi.org/10.1007/s00213-011-2446-6>.
- Blanco, E., Galeano, P., Palomino, A., Pavón, F.J., Rivera, P., Serrano, A., Alen, F., Rubio, L., Vargas, A., Castilla-Ortega, E., et al. (2016). Cocaine-induced behavioral sensitization decreases the expression of endocannabinoid signaling-related proteins in the mouse hippocampus. *Eur. Neuro-psychopharmacol* 26, 477–492. <https://doi.org/10.1016/j.euroneuro.2015.12.040>.
- Zhu, W., Mao, Z., Zhu, C., Li, M., Cao, C., Guan, Y., Yuan, J., Xie, G., and Guan, X. (2016). Adolescent exposure to cocaine increases anxiety-like behavior and induces morphological and neurochemical changes in the hippocampus of adult rats. *Neuroscience* 313, 174–183. <https://doi.org/10.1016/j.neuroscience.2015.11.041>.
- Bodas, D.S., Maduskar, A., Kaniganti, T., Wakhloo, D., Balasubramanian, A., Subhedar, N., and Ghose, A. (2023). Convergent Energy State-Dependent Antagonistic Signaling by Cocaine- and Amphetamine-Regulated Transcript (CART) and Neuropeptide Y (NPY) Modulates the Plasticity of Forebrain Neurons to Regulate Feeding in Zebrafish. *J. Neurosci.* 43, 1089–1110. <https://doi.org/10.1523/JNEUROSCI.2426-21.2022>.
- Tan, M., Luo, H., Lee, S., Jin, F., Yang, J.S., Montellier, E., Buchou, T., Cheng, Z., Rousseaux, S., Rajagopal, N., et al. (2011). Identification of 67 histone marks and histone lysine crotonylation as a new type of histone modification. *Cell* 146, 1016–1028. <https://doi.org/10.1016/j.cell.2011.08.008>.
- Ntorfa, A., and Burgoyne, J.R. (2021). The Regulation and Function of Histone Crotonylation. *Front. Cell Dev. Biol.* 9, 624914. <https://doi.org/10.3389/fcell.2021.624914>.
- Zhang, N., Yang, Z., Liang, W., and Liu, M. (2020). Global Proteomic Analysis of Lysine Crotonylation in the Plant Pathogen *Botrytis cinerea*. *Front. Microbiol.* 11, 564350. <https://doi.org/10.3389/fmicb.2020.564350>.
- Wang, R., Wang, Z., Wang, H., Pang, Y., and Lee, T.Y. (2020). Characterization and identification of lysine crotonylation sites based on machine learning method on both plant and mammalian. *Sci. Rep.* 10, 20447. <https://doi.org/10.1038/s41598-020-77173-0>.
- Liu, J.F., Wu, S.F., Liu, S., Sun, X., Wang, X.M., Xu, P., Chen, H.Z., and Yang, J.T. (2020). Global Lysine Crotonylation Profiling of Mouse Liver. *Proteomics* 20, e2000049. <https://doi.org/10.1002/pmic.202000049>.
- Hou, J.Y., Zhou, L., Li, J.L., Wang, D.P., and Cao, J.M. (2021). Emerging roles of non-histone protein crotonylation in biomedicine. *Cell Biosci.* 11, 101. <https://doi.org/10.1186/s13578-021-00616-2>.
- Sun, C.-F., Xu, W.-F., Zhao, Q.-W., Luo, S., Chen, X.-A., Li, Y.-Q., and Mao, X.-M. (2020). Crotonylation of key metabolic enzymes regulates carbon catabolite repression in *Streptomyces roseosporus*. *Commun. Biol.* 3, 192. <https://doi.org/10.1038/s42003-020-0924-2>.
- Gowans, G.J., Bridgers, J.B., Zhang, J., Dronamraju, R., Burnett, A., King, D.A., Thiengmany, A.V., Shinsky, S.A., Bhanu, N.V., Garcia, B.A., et al. (2019). Recognition of Histone Crotonylation by Taf14 Links Metabolic State to Gene Expression. *Mol. Cell* 76, 909–921.e3. <https://doi.org/10.1016/j.molcel.2019.09.029>.
- Sun, W., Liu, Q., Leng, J., Zheng, Y., and Li, J. (2015). The role of Pyruvate Dehydrogenase Complex in cardiovascular diseases. *Life Sci.* 121, 97–103. <https://doi.org/10.1016/j.lfs.2014.11.030>.
- Zhou, Z.H., McCarthy, D.B., O'Connor, C.M., Reed, L.J., and Stoops, J.K. (2001). The remarkable structural and functional organization of the eukaryotic pyruvate dehydrogenase complexes. *Proc. Natl. Acad. Sci. USA* 98, 14802–14807. <https://doi.org/10.1073/pnas.011597698>.
- Zhang, Y., Zhao, M., Gao, H., Yu, G., Zhao, Y., Yao, F., and Yang, W. (2022). MAPK signalling-induced phosphorylation and subcellular translocation of PDHE1 α promotes tumour immune evasion. *Nat. Metab.* 4, 374–388. <https://doi.org/10.1038/s42255-022-00543-7>.
- Cai, Z., Li, C.F., Han, F., Liu, C., Zhang, A., Hsu, C.C., Peng, D., Zhang, X., Jin, G., Rezaeian, A.H., et al. (2020). Phosphorylation of PDHA by AMPK Drives TCA Cycle to Promote Cancer Metastasis. *Mol. Cell* 80, 263–278.e7. <https://doi.org/10.1016/j.molcel.2020.09.018>.
- Fan, J., Shan, C., Kang, H.B., Elf, S., Xie, J., Tucker, M., Gu, T.L., Aguiar, M., Lonning, S., Chen, H., et al. (2014). Tyr phosphorylation of PDP1 toggles recruitment between ACAT1 and SIRT3 to regulate the pyruvate dehydrogenase complex. *Mol. Cell* 53, 534–548. <https://doi.org/10.1016/j.molcel.2013.12.026>.
- Jiang, G., Li, C., Lu, M., Lu, K., and Li, H. (2021). Protein lysine crotonylation: past, present, perspective. *Cell Death Dis.* 12, 703. <https://doi.org/10.1038/s41419-021-03987-z>.
- Li, H., Chen, R., Zhou, Y., Wang, H., Sun, L., Yang, Z., Bai, L., and Zhang, J. (2022). Endocannabinoids regulate cocaine-associated memory through brain AEA-CB1R signalling activation. *Mol. Metab.* 65, 101597. <https://doi.org/10.1016/j.molmet.2022.101597>.
- Shao, X., Tang, Y., Long, H., Gu, H., Zhang, J., Deng, P., Zhao, Y., and Cen, X. (2019). HMG-CoA synthase 2 drives brain metabolic reprogramming in cocaine exposure. *Neuropharmacology* 148, 377–393. <https://doi.org/10.1016/j.neuropharm.2017.10.001>.
- Bhandary, S., and Aguan, K. (2015). Pyruvate dehydrogenase complex deficiency and its relationship with epilepsy frequency—An overview. *Epilepsy Res.* 116, 40–52. <https://doi.org/10.1016/j.eplepsyres.2015.07.002>.
- Xu, S., Cheuk, Y.C., Jia, Y., Chen, T., Chen, J., Luo, Y., Cao, Y., Guo, J., Dong, L., Zhang, Y., et al. (2022). Bone marrow mesenchymal stem cell-derived exosomal miR-21a-5p alleviates renal fibrosis by attenuating glycolysis by targeting PFKM. *Cell Death Dis.* 13, 876. <https://doi.org/10.1038/s41419-022-05305-7>.

30. Pielage, J., Bulat, V., Zuchero, J.B., Fetter, R.D., and Davis, G.W. (2011). Hts/Adducin controls synaptic elaboration and elimination. *Neuron* 69, 1114–1131. <https://doi.org/10.1016/j.neuron.2011.02.007>.
31. Sabari, B.R., Tang, Z., Huang, H., Yong-Gonzalez, V., Molina, H., Kong, H.E., Dai, L., Shimada, M., Cross, J.R., Zhao, Y., et al. (2015). Intracellular crotonyl-CoA stimulates transcription through p300-catalyzed histone crotonylation. *Mol. Cell* 58, 203–215. <https://doi.org/10.1016/j.molcel.2015.02.029>.
32. Wei, W., Mao, A., Tang, B., Zeng, Q., Gao, S., Liu, X., Lu, L., Li, W., Du, J.X., Li, J., et al. (2017). Large-Scale Identification of Protein Crotonylation Reveals Its Role in Multiple Cellular Functions. *J. Proteome Res.* 16, 1743–1752. <https://doi.org/10.1021/acs.jproteome.7b00012>.
33. Tyssowski, K.M., DeStefino, N.R., Cho, J.H., Dunn, C.J., Poston, R.G., Carty, C.E., Jones, R.D., Chang, S.M., Romeo, P., Wurzelmann, M.K., et al. (2018). Different Neuronal Activity Patterns Induce Different Gene Expression Programs. *Neuron* 98, 530–546.e11. <https://doi.org/10.1016/j.neuron.2018.04.001>.
34. Zhang, Y., Xue, Y., Meng, S., Luo, Y., Liang, J., Li, J., Ai, S., Sun, C., Shen, H., Zhu, W., et al. (2016). Inhibition of Lactate Transport Erases Drug Memory and Prevents Drug Relapse. *Biol. Psychiatry* 79, 928–939. <https://doi.org/10.1016/j.biopsych.2015.07.007>.
35. Boury-Jamot, B., Carrard, A., Martin, J.L., Halfon, O., Magistretti, P.J., and Boutrel, B. (2016). Disrupting astrocyte-neuron lactate transfer persistently reduces conditioned responses to cocaine. *Mol. Psychiatry* 21, 1070–1076. <https://doi.org/10.1038/mp.2015.157>.
36. Natarajaseenivasan, K., Cotto, B., Shanmughapriya, S., Lombardi, A.A., Datta, P.K., Madesh, M., Elrod, J.W., Khalili, K., and Langford, D. (2018). Astrocytic metabolic switch is a novel etiology for Cocaine and HIV-1 Tat-mediated neurotoxicity. *Cell Death Dis.* 9, 415. <https://doi.org/10.1038/s41419-018-0422-3>.
37. Alavian, K.N., Li, H., Collis, L., Bonanni, L., Zeng, L., Sacchetti, S., Lazrove, E., Nabili, P., Flaherty, B., Graham, M., et al. (2011). Bcl-xL regulates metabolic efficiency of neurons through interaction with the mitochondrial F1FO ATP synthase. *Nat. Cell Biol.* 13, 1224–1233. <https://doi.org/10.1038/ncb2330>.
38. Ashrafi, G., Wu, Z., Farrell, R.J., and Ryan, T.A. (2017). GLUT4 Mobilization Supports Energetic Demands of Active Synapses. *Neuron* 93, 606–615.e3. <https://doi.org/10.1016/j.neuron.2016.12.020>.
39. Magistretti, P.J., and Allaman, I. (2018). Lactate in the brain: from metabolic end-product to signalling molecule. *Nat. Rev. Neurosci.* 19, 235–249. <https://doi.org/10.1038/nrn.2018.19>.
40. Mächler, P., Wyss, M.T., Elsayed, M., Stobart, J., Gutierrez, R., von Faber-Castell, A., Kaelin, V., Zuend, M., San Martín, A., Romero-Gómez, I., et al. (2016). In Vivo Evidence for a Lactate Gradient from Astrocytes to Neurons. *Cell Metab.* 23, 94–102. <https://doi.org/10.1016/j.cmet.2015.10.010>.
41. Baeza-Lehnert, F., Saab, A.S., Gutiérrez, R., Larenas, V., Díaz, E., Horn, M., Vargas, M., Hösl, L., Stobart, J., Hirrlinger, J., et al. (2019). Non-Canonical Control of Neuronal Energy Status by the Na(+) Pump. *Cell Metab.* 29, 668–680.e4. <https://doi.org/10.1016/j.cmet.2018.11.005>.
42. Du, F., Zhu, X.H., Zhang, Y., Friedman, M., Zhang, N., Ugurbil, K., and Chen, W. (2008). Tightly coupled brain activity and cerebral ATP metabolic rate. *Proc. Natl. Acad. Sci. USA* 105, 6409–6414. <https://doi.org/10.1073/pnas.0710766105>.
43. Suzuki, A., Stern, S.A., Bozdagi, O., Huntley, G.W., Walker, R.H., Magistretti, P.J., and Alberini, C.M. (2011). Astrocyte-neuron lactate transport is required for long-term memory formation. *Cell* 144, 810–823. <https://doi.org/10.1016/j.cell.2011.02.018>.
44. Chen, W., Sun, X., Zhan, L., Zhou, W., and Bi, T. (2021). Conditional Knockout of Pdha1 in Mouse Hippocampus Impairs Cognitive Function: The Possible Involvement of Lactate. *Front. Neurosci.* 15, 767560. <https://doi.org/10.3389/fnins.2021.767560>.
45. Liu, L., Cao, J., Zhao, J., Li, X., Suo, Z., and Li, H. (2019). PDHA1 Gene Knockout In Human Esophageal Squamous Cancer Cells Resulted In Greater Warburg Effect And Aggressive Features In Vitro And In Vivo. *Oncotargets Ther.* 12, 9899–9913. <https://doi.org/10.2147/OTT.S226851>.
46. Mo, F., Zhang, H., Tang, Y., Qi, R., Nie, S., Shen, H., and Li, M. (2021). Pyruvate accumulation may contribute to acceleration-induced impairment of physical and cognitive abilities: an experimental study. *Biosci. Rep.* 41, BSR20204284. <https://doi.org/10.1042/BSR20204284>.
47. Yu, H., Bu, C., Liu, Y., Gong, T., Liu, X., Liu, S., Peng, X., Zhang, W., Peng, Y., Yang, J., et al. (2020). Global crotonylome reveals CDYL-regulated RPA1 crotonylation in homologous recombination-mediated DNA repair. *Sci. Adv.* 6, eaay4697. <https://doi.org/10.1126/sciadv.aay4697>.
48. Jha, M.K., Lee, I.K., and Suk, K. (2016). Metabolic reprogramming by the pyruvate dehydrogenase kinase-lactic acid axis: Linking metabolism and diverse neuropathophysiology. *Neurosci. Biobehav. Rev.* 68, 1–19. <https://doi.org/10.1016/j.neubiorev.2016.05.006>.
49. Liu, C., Sun, X., Wang, Z., Le, Q., Liu, P., Jiang, C., Wang, F., and Ma, L. (2018). Retrieval-Induced Upregulation of Tet3 in Pyramidal Neurons of the Dorsal Hippocampus Mediates Cocaine-Associated Memory Reconsolidation. *Int. J. Neuropsychopharmacol.* 21, 255–266. <https://doi.org/10.1093/ijnp/pyx099>.
50. Wells, A., Xie, X., Higginbotham, J., Arguello, A., Healey, K., Blanton, M., and Fuchs, R. (2016). Contribution of an SFK-Mediated Signaling Pathway in the Dorsal Hippocampus to Cocaine-Memory Reconsolidation in Rats. *Neuropsychopharmacology* 41, 675–685. <https://doi.org/10.1038/npp.2015.217>.
51. Adinoff, B., Gu, H., Merrick, C., McHugh, M., Jeon-Slaughter, H., Lu, H., Yang, Y., and Stein, E.A. (2015). Basal Hippocampal Activity and Its Functional Connectivity Predicts Cocaine Relapse. *Biol. Psychiatry* 78, 496–504. <https://doi.org/10.1016/j.biopsych.2014.12.027>.
52. Park, A., Jacob, A.D., Hsiang, H.L., Frankland, P.W., Howland, J.G., and Josselyn, S.A. (2023). Formation and fate of an engram in the lateral amygdala supporting a rewarding memory in mice. *Neuropsychopharmacology* 48, 724–733. <https://doi.org/10.1038/s41386-022-01472-5>.
53. Hsiang, H.L., Epp, J.R., van den Oever, M.C., Yan, C., Rashid, A.J., Insel, N., Ye, L., Niibori, Y., Deisseroth, K., Frankland, P.W., and Josselyn, S.A. (2014). Manipulating a "cocaine engram" in mice. *J. Neurosci.* 34, 14115–14127. <https://doi.org/10.1523/JNEUROSCI.3327-14.2014>.
54. Liu, X., Ramirez, S., Pang, P.T., Puryear, C.B., Govindarajan, A., Deisseroth, K., and Tonegawa, S. (2012). Optogenetic stimulation of a hippocampal engram activates fear memory recall. *Nature* 484, 381–385. <https://doi.org/10.1038/nature11028>.
55. Leutgeb, J.K., and Moser, E.I. (2007). Enigmas of the dentate gyrus. *Neuron* 55, 176–178. <https://doi.org/10.1016/j.neuron.2007.07.002>.
56. Cumming, B.M., Addicott, K.W., Adamson, J.H., and Steyn, A.J. (2018). Mycobacterium tuberculosis induces decelerated bioenergetic metabolism in human macrophages. *Elife* 7, e39169. <https://doi.org/10.7554/eLife.39169>.
57. Wang, Y.Q., Wang, H.L., Xu, J., Tan, J., Fu, L.N., Wang, J.L., Zou, T.H., Sun, D.F., Gao, Q.Y., Chen, Y.X., and Fang, J.Y. (2018). Sirtuin5 contributes to colorectal carcinogenesis by enhancing glutaminolysis in a deglutaryl-dependent manner. *Nat. Commun.* 9, 545. <https://doi.org/10.1038/s41467-018-02951-4>.
58. Li, H., Wan, X., Wu, Z., Zhou, Y., Chen, R., Xu, W., Zhang, J., Yang, Z., Bai, L., Zhang, J., et al. (2022). β -hydroxybutyrate reduces reinstatement of cocaine conditioned place preference through hippocampal CaMKII- α β -hydroxybutyrylation. *Cell Rep.* 41, 111724. <https://doi.org/10.1016/j.celrep.2022.111724>.

STAR★METHODS

KEY RESOURCES TABLE

REAGENT or RESOURCE	SOURCE	IDENTIFIER
Antibodies		
Rabbit anti-Pan Kcr (1:1000)	PTM Biolabs	Cat# PTM-501
Rabbit anti-PDHA1 (1:1000)	Abcam	Cat# ab_168379
Rabbit anti-H3 (1:1000)	Abcam	Cat# ab_12079
Rabbit anti-GAPDH (1:2000)	YEASEN	Cat# 30202ES60
Rabbit anti- β -adducin (1:1000)	Proteintech	Cat# 14640-1-AP
Rabbit anti-PFKM (1:1000)	Abcam	Cat# 13-7300
Rabbit anti-P300 (1:1000)	Abcam	Cat# ab_275378
Rabbit anti-HDAC1 (1:1000)	Proteintech	Cat# 10197-1-AP
Rabbit anti-HDAC2 (1:1000)	Proteintech	Cat# 12922-3-AP
Rabbit anti-HDAC3 (1:1000)	Proteintech	Cat# 10255-1-AP
Rabbit anti-pS 293 (1:1000)	Abcam	Cat# ab_177461
Mouse anti-c-Fos (1:1000)	Abcam	Cat# ab_214672
Rabbit anti-Arc (1:1000)	Abcam	Cat# ab_177461
Rabbit anti-K39 Cr (1:1000)	PTM biolabs	N/A
Mouse anti-Flag (1:1000)	YEASEN	Cat# 30505ES60
Rabbit anti-c-Fos (1:100 for IHC; 1:400 for IF)	CST	Cat# 31254S
Mouse anti-PDHA1 (1:200 for IHC)	Abcam	Cat# ab_110330
Rabbit anti-CaMKII- α (1:100 for IHC)	Proteintech	Cat# 13730-1-AP
Donkey anti-rabbit Alexa Fluor 568 (1:200)	Invitrogen	Cat# A-10042
Donkey anti-rabbit Alexa Fluor 647(1:500)	Invitrogen	Cat# A-31573
Donkey anti-mouse Alexa Fluor 488 (1:200)	Invitrogen	Cat# A-21202
Goat anti-mouse HRP (1:2000)	Invitrogen	Cat# C31430100
Goat anti-rabbit HRP (1:2000)	Invitrogen	Cat# C31460100
Bacterial and virus strains		
AAV2/9-CaMKII-hM3Dq-mCherry	Obio Technology	N/A
AAV2/8-CaMKII-hM4Di-mCherry	Obio Technology	N/A
AAV2/8-CaMKII-EGFP-2A-cre	Obio Technology	N/A
AAV2/8-CaMKII-PDHA1-Flag	Obio Technology	N/A
AAV2/8-CaMKII-mutant PDHA1-Flag	Vigene Biotechnology	N/A
pSLenti-U6-shRNA PDHA1-CMV-EGFP-2A-Puro	Vigene Biotechnology	N/A
pSLenti-U6-shRNA P300-CMV-EGFP-2A-Puro	Vigene Biotechnology	N/A
pLenti-EF1a-mCherry-2A-blasticidin-CMV-PDHA1-Flag	Vigene Biotechnology	N/A
pLenti-EF1a-mCherry-2A-blasticidin-CMV-mutant PDHA1-Flag	Vigene Biotechnology	N/A
Chemicals, peptides, and recombinant proteins		
Cocaine	National Institute for the Control of Pharmaceutical and Biological Products	N/A
Croconic acid disodium	Sigma-Aldrich	Cat# 391719
Acetic acid sodium	Sigma-Aldrich	Cat# S2889
Tamoxifen	Sigma-Aldrich	Cat# 579002
A485	Selleck Chemicals	Cat# S8740
Clozapine-N-oxide	Selleck Chemicals	Cat# S6887
DMEM/High glucose Medium	Gibco	Cat# C1195500BT

(Continued on next page)

Continued		
REAGENT or RESOURCE	SOURCE	IDENTIFIER
Fetal bovine serum	Gibco	Cat# 10099-141
Antibiotic-Antimycotic	Gibco	Cat# 15240-062
Phosphatase inhibitors	Roche	Cat# 4906845001
PBS	Hyclone	Cat# 10010049
¹³ C-labeled pyruvate	Cambridge Isotope Laboratories	Cat# CLM-1575
Anti-fade mounting medium	Vector	Cat# H-1000
Recombinant human PDHA1 Protein	Abcam	Cat# ab_125602
Recombinant human P300 Protein	Abcam	Cat# ab_56274
Chemiluminescence substrate	Millipore	Cat# WBKLS0500
Protein A/G magnetic beads	Bimake	Cat# B23201
Anti-Flag beads	Bimake	Cat# B26101
Flag peptide	Bimake	Cat# B23111
Crotonoyl-CoA trillithium salt	Sigma-Aldrich	Cat# 28007
Critical commercial assays		
HDAC Activity Fluorometric Assay Kit	Biovision	Cat# K330-100
Mammalian Cell & Tissue Extraction Kit	Biovision	Cat# K269-500
Bradford assay kit	Beyotime	Cat# P0006
PDH enzyme activity microplate assay kit	Abcam	Cat# ab_109902
Pierce™ Crosslink Magnetic IP/co-IP Kit	Thermo	Cat# 88805
pyruvate colorimetric/fluorometric assay kit	Biovision	Cat# K609
acetyl-CoA fluorometric assay kit	Biovision	Cat# K317
ATP colorimetric/fluorometric assay kit	Biovision	Cat# K354
Creatine colorimetric/fluorometric assay kit	Biovision	Cat# K635
ADP colorimetric assay kit	Biovision	Cat# K356
10 kDa molecular weight cut off spin columns	Beyotime	Cat# FUF051
P300 Inhibitor Screening Assay Kit	Beyotime	Cat# K346-100
Deposited data		
Identified Kcr peptides (see also Table S1)	ProteomeXchange	PXD053497
Experimental models: cell lines		
HT22 cells	Pricella	Cat# CL-0697
Experimental models: organisms/strains		
Mouse: Adult C57BL6/J	Charles River	N/A
Mouse: PDHA1-floxed mice	GemPharmatech Company	T009249
Mouse: CaMKII-cre ERT2 ^{+/-} mice	GemPharmatech Company	N/A
Software and algorithms		
UniProt-GOA database	UniPort	http://www.ebi.ac.uk/GOA/
UniProt database	UniPort	http://www.uniprot.org
GraphPad Prism 7.0	GraphPad Software	http://www.graphpad.com/
Chemi Analysis software	CLINX	N/A
Nis-Elements	Nikon	www.microscope.healthcare.nikon.com
Celigo Imaging Cytometer	Nexcelom Bioscience	N/A
Agilent 5975 C inert MSD system	Agilent Technologies Inc	N/A
CELLO	N/A	http://cello.life.nctu.edu.tw/
MoMo	N/A	http://motif-x.med.harvard.edu/
Wolfsort	WoLF PSORT	https://wolfsort.hgc.jp/
STRING database (version 10.1)	STRING	https://cn.string-db.org/
Other		
Guide cannula	RWD	Cat#800-00185-00
Stainless-steel cap	RWD	Cat#800-00241-00

RESOURCES AVAILABILITY

Lead contact

Further information and requests for resources and reagents should be directed to and will be fulfilled by the lead contact, Xiaobo Cen (xbcen@scu.edu.cn).

Materials availability

Our study did not generate any new unique reagents.

Data and code availability

The mass spectrometry proteomics data have been deposited at the ProteomeXchange Consortium via the PRIDE partner repository with the dataset identifier ProteomeXchange: PXD053497 and are publicly available as of the date of publication. Accession numbers are listed in the [key resources table](#). The hippocampal proteomics analysis of kbhb data are also available in [Table S1](#).

This paper does not report original code.

Any additional information required to reanalyze the data reported in this paper is available from the [lead contact](#) upon request.

EXPERIMENTAL MODEL AND STUDY PARTICIPANT DETAILS

Animals

Male C57BL/6J wild-type (WT) mice were purchased from Vital River Laboratory Animal Technology Co., Ltd. (Beijing, China), and the mice aged 8–12 weeks were used in this study. PDHA1-floxed (PDHA1^{fl/fl}) mice were supplied by GemPharmatech Company (T009249, Nanjing, China). CaMKII-cre ERT2^{+/-} mice with a C57BL/6J background expressing excitatory neuron-specific cre topoisomerase were provided by GemPharmatech Company (Nanjing, China). All mice were housed in the animal room on a standard 12-h light/12-h dark cycle with a constant temperature and food and water available *ad libitum*. All experimental procedures and use of the animals were conducted in accordance with the guidelines established by the Association for Assessment and Accreditation of Laboratory Animal Care and the Institutional Animal Care and Use Committee of Sichuan University (20220225132). All efforts were made to minimize the suffering of the mice.

Excitatory neuron-specific PDHA1-deficient mice were obtained by breeding PDHA1-floxed mice with CaMKII-cre ERT2^{+/-} mice. To delete PDHA1 in excitatory neurons of the brain, the mice were intraperitoneally injected with tamoxifen (dissolved in corn oil at a concentration of 2.5 mg/mL) once a day for five successive days at a daily dose of 100 mg/kg.

Cell lines

HT22 cells, an immortalized mouse hippocampal cell line, were cultured in Dulbecco's Modified Eagle's Medium with high glucose (DMEM, C1195500BT, Gibco) containing 10% fetal bovine serum (10099–141, Gibco), penicillin (100 U/mL) and streptomycin (100 µg/mL) (15240–062, Gibco) and grown in a 5% CO₂ atmosphere at 37°C.

Drugs

Cocaine was purchased from the National Institute for the Control of Pharmaceutical and Biological Products (Beijing, China) and dissolved in saline. A485 (S8740, Selleck Chemicals) and clozapine-N-oxide (CNO, S6887, Selleck Chemicals) were purchased from Selleck Chemicals. Tamoxifen (579002, Sigma–Aldrich) and croconic acid disodium (391719, Sigma–Aldrich) and acetic acid sodium (S2889, Sigma–Aldrich) were purchased from Sigma–Aldrich.

METHOD DETAILS

Clozapine-N-oxide (CNO) administration

Mice were pretreated with CNO according to the timelines shown in the figures. To decrease dDG granule cell activity, mice expressing AAV2/8-CaMKII-hM4Di-mCherry in the dDG were injected intraperitoneally with CNO (5 mg/kg) 30 min before the CPP test or CPP training. To excite dDG granule cell activity, mice expressing AAV2/9-CaMKII-hM₃Dq-mCherry in the dDG were injected intraperitoneally with CNO (0.2 mg/kg) 30 min before the CPP test or CPP training (see section entitled '[Viral injections](#)' for details).

Behavioral paradigm

Mice were acclimated to the laboratory environment for one week before the experiments and habituated to handling for 2 d before each behavioral test. Conditioned place preference (CPP) was used to assess cocaine-associated memory formation. Food CPP, home-cage cocaine injection, and locomotor activity and contextual fear conditioning were also employed. All behavioral experiments were performed in a double-blind manner.

CPP

The CPP test was conducted using a standard three-chambered apparatus equipped with two large conditioning compartments (black and white) that differed in their flooring (bar and grid) and a small middle chamber (gray, with a smooth PVC floor) that connected the two large compartments. Before each session, the mice were habituated to the chambers for at least 10 min per day on 2 consecutive days.

Pretest session

The baseline preference was assessed by placing the mice in the middle chamber and allowing them to explore all three chambers freely for 15 min. The baseline preference was calculated by subtracting the time spent in the black chamber from the time spent in the white chamber ($\text{Time}_{\text{pre test}}$). Mice were excluded from the CPP training if they showed a strong unconditioned preference for either side chamber (chamber bias >300 s or chamber bias <-300 s).

CPP training

Mice were randomly divided into two groups and trained for 6 d with alternating injections of cocaine (20 mg/kg or 2.5 mg/kg, *i.p.*) and saline. Cocaine-treated mice were immediately placed into the cocaine-paired chamber for 30 min after cocaine injection. On the following day, these mice received a saline injection and were immediately placed into the opposite chamber for 30 min. Saline-treated mice received an injection of saline and were placed into the saline-paired chamber for 30 min. On the following day, these mice received another saline injection and were placed in the opposite chamber for 30 min. The alternating sessions of conditioning were repeated until 3 cycles were completed (a total of 6 d).

CPP test

On the day of the CPP test, the animals were placed in the middle compartment, and the time spent in the two compartments was recorded for 15 min. We defined the time spent in the black chamber minus the time spent in the white chamber as $\text{Time}_{\text{test}}$. The CPP score was calculated as the $\text{Time}_{\text{test}}$ minus the $\text{Time}_{\text{pre test}}$ ($\text{CPP score} = \text{Time}_{\text{test}} - \text{Time}_{\text{pre test}}$). In general, cocaine results in a positive CPP score and strongly reverses any preference to the contrary; the CPP score was defined as the extent of the shift in preference after cocaine injection.

Food CPP

The apparatus and methodology for the food CPP test were similar to those described above for cocaine CPP. Mice were food-restricted for one week before the test; their weight was maintained at 80% of their original body weight. During the food conditioning sessions, the food conditioning group was transferred to the food-paired chamber (2–3 g of food was placed in the chamber) for 30 min. In the non-food conditioning sessions, mice were assigned to the nonfood-paired chamber for 30 min. Outside conditioning training, animals had access to food only once daily for 1 h after the training session ended. The alternating sessions of conditioning were repeated via 3 cycles (a total of 6 d). On the day of the test, mice were placed in the central chamber and allowed to freely explore all three chambers for a total of 15 min; the time spent in each chamber was recorded to calculate the CPP score.

Home cage cocaine injection

Mice were treated with cocaine as described for cocaine CPP training but were not confined to the drug-paired chamber or the unpaired chamber after drug injection; instead, they were returned to their home cages without any exposure to the test apparatus. On the day of the CPP test, the mice were placed in the central chamber and allowed to freely explore all three chambers for a total of 15 min; the time spent in each chamber was recorded to evaluate the CPP score.

Locomotor activity

Locomotor activity was measured as the distance traveled. Mice were acclimated to chambers (48 × 48 cm) equipped with a camera for 15 min once a day for 2 consecutive days. Before the test, the baseline locomotor activity was not significantly different between each group. In the following week, mice were injected with cocaine (20 mg/kg, *i.p.*) or an equal volume of saline, immediately placed in the locomotor activity chamber, and allowed to explore for 15 min. Automated tracking was performed with EthoVision 7.0 software (EthoVision 7.0; Noldus Information Technology), and the distance traveled by the mice was measured daily for one week.

Contextual fear conditioning

The chamber used for contextual fear conditioning had lights and a grid floor consisting of 24 stainless steel rods. The mice were kept in the conditioning context A chamber for a total of 300 s during the training period, and foot shocks (2 s, 0.75 mA) were applied at 120, 180, and 240 s. The mice were placed in the chamber and permitted to explore for 180 s to observe their freezing behavior on the next morning. Contextual fear memory was assessed by manually evaluating freezing behavior; freezing was defined as the absence of movement for at least 2 s. The freezing time in chamber was recorded to evaluate fear behavior.

Stereotactic surgery and drug administration

Mice were anesthetized with sodium pentobarbital (60 mg/kg) and mounted in a standard stereotaxic instrument (RWD Life Science). The hair was shaved from the planned incision site on the scalp, and the site was cleaned with medical-grade alcohol. The scalp was incised to expose the skull, and permanent bilateral guide cannulas were implanted into the dDG (AP, -2.0 mm; ML, ± 1.4 mm; DV, -2.2 mm) with stereotaxic instruments. Dental cement was used to anchor the guide cannula, and a stainless-steel stylet was left in each cannula to prevent blockage and infection. All mice began cocaine CPP training after one week of recovery from surgery. Croconic acid disodium was dissolved in saline at a final concentration of $3.7 \mu\text{g}/\mu\text{L}$ and was administered bilaterally ($1 \mu\text{L}/\text{side}$, $0.5 \mu\text{L}/\text{min}$) with a microinjector 30 min before cocaine or saline administration during cocaine-associated memory formation.

Stereotactic surgery and adeno-associated virus injection

Mice (aged 8–12 weeks) were anesthetized with sodium pentobarbital (60 mg/kg) and fixed on a stereotaxic apparatus. Small craniotomy holes were drilled with a skull rotor (RWD Life Science) for virus injection. Virus was injected bilaterally into the dDG (AP, -2.0 mm; ML, ± 1.4 mm; DV, -2.2 mm). After each injection, the needle was left at the injection site of the brain for an additional 5 min to aid diffusion from the needle tip and to prevent backflow. The needle was then slowly retracted, and the scalp incision was closed with sutures. Mice were housed for 3 weeks postoperatively before the start of CPP training to allow recovery from surgery and sufficient viral expression. For *in vivo* regulation of dDG neuron activity, AAV2/9-CaMKII-hM₃Dq-GFP or AAV2/8-CaMKII-hM₄D_i-GFP virus (Obio Technology Co Ltd) was bilaterally injected into the dDG ($0.5 \mu\text{L}/\text{side}$) of mice at a constant speed of $0.1 \mu\text{L}/\text{min}$.

For *in vivo* exploration of the role of PDHA1 K39 Cr in cocaine-associated memory formation, AAV2/8-CaMKII-EGFP-cre and AAV2/8-CaMKII-PDHA1-Flag were constructed by Obio Technology Co., Ltd. (Shanghai, China), and AAV2/8-CaMKII-mutant PDHA1-Flag was constructed by Vigene Biotechnology Co. (Jinan, China). Point mutations of lysine 39 to alanine 39 were synthesized in the murine full-length PDHA1 amino acid sequence. AAV2/8-CaMKII-EGFP-cre ($0.5 \mu\text{L}$, $0.1 \mu\text{L}/\text{min}$), AAV2/8-CaMKII-PDHA1-Flag ($0.5 \mu\text{L}$, $0.1 \mu\text{L}/\text{min}$) or AAV2/8-CaMKII-mutant PDHA1-Flag ($0.5 \mu\text{L}$, $0.1 \mu\text{L}/\text{min}$) were infused into the bilateral hippocampal dDG region (AP, -2.0 mm; ML, ± 1.4 mm; DV, -2.2 mm).

Lentiviral vector construction and cell transfection

The lentiviral vectors (LVs): pSLenti-U6-shRNA P300-CMV-EGFP-2A-Puro (the sequences of the scrambled control shRNA and P300 shRNA were $5'$ -TTCTCCGAACGTGTCACGT- $3'$ and $5'$ -GCAATGGACAAGGGATAATTT- $3'$, respectively). pSLenti-U6-shRNA PDHA1-CMV-EGFP-2A-Puro (the sequences of the scrambled control shRNA and PDHA1 shRNA were $5'$ -CCTAAGGT-TAAGTCGCCCTCG- $3'$ and $5'$ -GCTCAAGTACTACAGGATGAT- $3'$, respectively). The shRNA PDHA1-resistant forms of FLAG tag PDHA1 and mutant PDHA1 (the sequences of $5'$ -GCTCAAGTACTACAGGATGAT- $3'$ was mutated $5'$ -GCTGAAATATTATCGCATGAT- $3'$). These LVs were constructed by Vigene Biotechnology Co. (Jinan, China) for cell studies.

DMEM was replaced with serum-free DMEM and incubated for 2 h before transfection, and this step was followed by incubation with the lentiviral vector containing PDHA1-shRNA. Antibiotic-resistant clones were selected with $2.5 \mu\text{g}/\text{mL}$ puromycin. PDHA1-knockdown cells were transfected with a lentiviral vector containing PDHA1-shRNA-resistant PDHA1 or mutant PDHA1. Antibiotic-resistant clones were picked and cultured in DMEM containing $10 \mu\text{g}/\text{mL}$ blasticidin. Purified Flag-PDHA1 or Flag-mutant PDHA1 was extracted from transfected HT22 cells. Western blotting analysis was performed with antibodies specific for PDHA1 K39 Cr.

Tissue isolation

Mice were sacrificed by rapid decapitation at the end of the behavioral tests. Hippocampal dDG tissue was separately removed from the mouse brain, snap-frozen on dry ice, and stored at -80°C until assayed.

Western blot

After brain tissues and cells were lysed, proteins were extracted using a mammalian cell and tissue extraction kit (K269-500, BioVision) containing phosphatase inhibitors (4906845001, Roche). The total protein concentration was detected with a Bradford assay kit (P0006, Beyotime). Protein (20 mg) was loaded and separated with a 10% or 4–20% sodium dodecyl sulfate polyacrylamide gel. After loading, the gels were then transferred to the polyvinylidene difluoride (PVDF) membrane. Membrane was blocked in TBST buffer containing 5% non-fat dry milk for 1 h at room temperature, and then incubated and gently shaken overnight with primary antibody at 4°C . The membrane was incubated with secondary antibody at room temperature for 2 h, and protein immunoreactivity was visualized using a chemiluminescence substrate (WBKLS0500, Millipore). The following antibodies were used for Western blotting: rabbit anti-Pan crotonyllysine (Pan-Kcr, 1:1000, PTM Bio), rabbit anti-PDHA1 (1:1000, Abcam), rabbit anti- β -adducin (1:1000, Proteintech), rabbit anti-PFKM (1:1000, Abcam), rabbit anti-H3K9cr (1:1000, PTM Bio), rabbit anti-H3K14cr (1:1000, PTM Bio), mouse anti-H3K18cr (1:1000, PTM Bio), rabbit anti-H3 (1:1000, Abcam), rabbit anti-P300 (1:1000, Abcam), rabbit anti-HDAC1 (1:1000, Proteintech), rabbit anti-HDAC2 (1:1000, Proteintech), rabbit anti-HDAC3 (1:1000, Proteintech), mouse anti-Flag (1:1000, YEASEN), mouse anti-c-Fos (1:1000, Abcam), rabbit anti-K39 Cr (1:1000, PTM Bio), rabbit anti-GAPDH (1:2000, YEASEN), goat anti-mouse HRP (1:2000, Invitrogen) and goat anti-rabbit HRP (1:2000, Invitrogen).

Co-immunoprecipitation

To clarify whether PDHA1, β -adducin and PFKM are targets of lysine crotonylation, cells or tissues were harvested for coimmunoprecipitation (co-IP) analysis using the simplified and reliable Pierce Crosslink Magnetic IP/co-IP Kit (88805, Thermo Scientific). Briefly, anti-PDHA1, β -adducin or PFKM primary antibody was bound to 50 mL of Protein A/G magnetic beads (B23201, Bimake) for 15 min and washed three times. The protein was extracted using the mammalian cell and tissue extraction kit (K269-500, BioVision), and the protein supernatant from each sample was incubated with the antibody-crosslinked beads overnight at 4°C, the beads were washed twice with IP lysis/wash buffer, and the supernatants were collected for western blotting analysis.

Western blotting analysis of PDHA1, β -adducin and PFKM lysine crotonylation

The hippocampal tissues and cells were lysed with a mammalian cell and tissue extraction kit (K269-500, BioVision). PDHA1, β -adducin and PFKM Kcr were purified by IP with PDHA1, β -adducin and PFKM primary antibodies, and Kcr was detected by western blotting using Pan-Kcr antibodies (PTM-501, PTM Bio). The band optical density was quantified using Chemi Analysis software (CLINX, Shanghai, China). The PDHA1, β -adducin and PFKM levels were used as controls to quantify the PDHA1, β -adducin and PFKM Kcr levels.

Enzymatic assay of PDH activity

A PDH enzyme activity microplate assay kit (ab109902, Abcam) was used to measure PDH activity in brain tissues and HT22 cells. Brain tissues or cells were homogenized to determine the protein concentrations by a Bradford Protein Assay kit (P0006, Beyotime), and supernatants were used for the PDH assay according to the manufacturer's protocol. Briefly, tissue or cells (2×10^6) were homogenized with ice-cold assay buffer and then incubated on ice for 10 min. The samples were measured in a 96-well plate at 450 nm in kinetic mode for 0–60 min at room temperature. PDH activity was calculated according to the manufacturer's instructions.

Pyruvate metabolite assays

Extracts from mouse brain tissues or HT22 cells were used for quantitative measurement of pyruvate metabolites, including pyruvate, acetyl-CoA, ATP, creatine and ADP. The levels of the metabolites were determined using a pyruvate colorimetric/fluorometric assay kit (K609, BioVision), acetyl-CoA fluorometric assay kit (K317, BioVision), ATP colorimetric/fluorometric assay kit (K354, BioVision), creatine colorimetric/fluorometric assay kit (K635, BioVision), and ADP colorimetric assay kit (K356, BioVision). Briefly, tissue or 2×10^6 cells were lysed in the corresponding assay buffer. After samples were deproteinized using 10-kDa molecular weight cut off spin columns (FUF051, Beyotime), a specific reaction was performed, and the absorption/fluorescence was measured according to the manufacturer's instructions.

Seahorse assay

A bioenergetic analysis of HT22 cells was performed using a Seahorse XF24 extracellular flux analyzer (Agilent). Briefly, HT22 cells were seeded into XF24 plates 24 h before the assay. For the OCR analysis, the cells were washed twice with the XF Assay medium and then incubated at 37°C in a CO₂-free incubator to allow temperature and pH equilibration. After 1 h, the cells were loaded into the XF analyzer. Oligomycin A (50 μ M) and FCCP (30 μ M) were applied to each well sequentially to measure the basal and maximal oxygen consumption, and a mixture of antimycin A and rotenone (10 μ M/each) was applied to measure nonmitochondrial respiration. After the Seahorse assay, the number of HT22 cells was counted manually using a Celigo Imaging Cytometer (Nexcelom Bioscience), the values of OCR were normalized to the cell number, and the parameter calculation of OCR was performed according to previous studies.⁵⁶

¹³C-labeled pyruvate tracing

For the ¹³C-labeled pyruvate tracing assay, the cells were treated with 2 mM ¹³C-labeled pyruvate (CLM-1575, Cambridge Isotope Laboratories) for 6 h and then subjected to methanol extraction to prepare samples according to previously published methods.^{23,57} Briefly, after treatment with ¹³C-labeled pyruvate, HT22 cells (2×10^6 /sample) were rinsed with 37°C PBS. The cell sample was immediately added to 1 mL of methanol:H₂O (8:2, V/V, –75°C, on dry ice) and incubated for 30 min at –75°C to quench metabolism and perform extraction. Cells were scraped from the flask at –75°C and transferred into tubes. The mixture was centrifuged at 13,000 rpm for 5 min at 4°C to remove all the soluble extract. Pyruvate metabolites were derivatized with methoxyamine (15 mg/mL in pyridine) for 90 min at 37°C and subsequently with N-(tert-butylidimethylsilyl)-N-methyltrifluoroacetamide at 55°C for 60 min.

¹³C-labeled pyruvate tracing analysis was performed using an Agilent 7890A gas chromatography system coupled to an Agilent 5975 C inert MSD system (Agilent Technologies Inc., CA, USA). An HP-5ms fused-silica capillary column (30 m \times 0.25 mm \times 0.25 μ m; Agilent J&W Scientific, Folsom, CA, USA) was utilized to separate the derivatives. Mass spectra were collected at m/z 50–600 under the selected reaction monitoring mode.

For stable isotope-tracing analysis of intracellular pyruvate metabolites, the measured distribution of mass isotopomers was corrected for the natural abundance of isotopes using IsoCor software. The labeled metabolite data are expressed using the percentage of the total pool or relative ion abundances. The pyruvate metabolite levels were determined by normalization to the internal standard and cell number from parallel flasks.

Immunohistochemistry

Mice that had undergone behavioral training were anesthetized with sodium pentobarbital (60 mg/kg), perfused transcardially with PBS, and treated with 4% paraformaldehyde (PFA) in 0.1 M PBS (pH 7.4). Brains were sectioned into 45- μ m coronal slices using a freezing microtome (Leica) and stored in 12-well plates filled with a cryoprotectant solution at -20°C until processing for immunohistochemical staining. The sections were incubated with blocking solution containing 0.3% Triton X-100 and 5% normal donkey serum in TBS for 2 h at room temperature. The sections were then incubated with primary antibodies in blocking solution at 4°C overnight. The sections were transferred to blocking solution containing fluorescent dye-conjugated secondary antibodies and then incubated for 1.5 h. The sections were stained with DAPI for 5 min and mounted with antifade mounting medium containing DAPI (H-1000, Vector), and confocal images were acquired with a laser confocal microscope (Nikon). The corresponding dDG area and c-Fos fluorescence intensity were determined using ImageJ software (National Institutes of Health) to assess the c-Fos fluorescence intensity in the dDG. The following antibodies were used for immunostaining: rabbit anti-c-Fos (1:100, CST) and donkey anti-rabbit Alexa Fluor 568 (1:200, Invitrogen).

The c-Fos fluorescence intensity was measured using ImageJ (NIH) by selecting regions of interest (ROIs). For IHC, the hippocampal dDG was identified by DAPI staining of the cells. The ROI contained the whole dDG. The c-Fos density was calculated by dividing the c-Fos fluorescence intensity by the ROI area (μm^2). Approximately 5 sections of the dDG were analyzed for each animal. A total of 15 sections from three independent mice per group were analyzed. To quantify the c-Fos fluorescence intensity in the dDG (fluorescence intensity/dDG), we first measured the area of each section by using ImageJ software and then calculated the c-Fos fluorescence intensity.

Immunocytochemistry

Cells cultured on glass coverslips were fixed with 4% PFA for 10 min. After three washes with PBS, the cells were blocked with blocking buffer for 1 h and then incubated with primary antibodies overnight. The coverslips were incubated with fluorescent dye-conjugated secondary antibodies for 1 h at room temperature. The coverslips were stained with DAPI for 5 min and mounted with anti-fade mounting medium (H-1000, Vector). The following antibodies were used for immunostaining: rabbit anti-c-Fos (1:400, CST) and Alexa Fluor 647-conjugated donkey anti-rabbit (1:500, Invitrogen). For *in vitro* experiments, the ROIs were determined in the captured images. The fluorescence intensity of c-Fos was calculated by dividing the fluorescence intensity by the ROI area (in μm^2) using ImageJ software. Six sections of the dDG were analyzed for each coverslip. A total of 18 sections from three independent coverslips per group were analyzed.

PDHA1 crotonylation *in vitro*

An *in vitro* assay to induce Kcr of PDHA1 was performed as described previously with minor modification.⁵⁸ Reactions were set up in reaction buffer (25 mM Tris-HCl pH 8.0, 100 mM NaCl, 1 mM DTT, 100 mM EDTA, 10% glycerol, supplemented with Protease Inhibitor Cocktail, 10 mM nicotinamide and 100 ng/mL TSA) with 10 μg of recombinant PDHA1 (ab125602, Abcam) and 10 mM crotonoyl-CoA trilithium salt (28007, Sigma-Aldrich) for 2 h in 37°C water bath. The reactions were stopped by the addition of SDS loading buffer for western blotting measurement.

P300-catalyzed PDHA1 crotonylation *in vitro*

An *in vitro* assay was performed to confirm whether P300 induced Kcr of PDHA1. 10 micrograms of recombinant P300 (ab56274, Abcam), 10 μg of recombinant PDHA1 and 10 mM crotonoyl-CoA trilithium salt were incubated in reaction buffer (25 mM Tris-HCl pH 8.0, 100 mM NaCl, 1 mM DTT, 100 mM EDTA, 10% glycerol, 10 mM nicotinamide and 100 ng/mL TSA) for 3 h in a 37°C water bath. The reactions were stopped by the addition of SDS loading buffer for western blotting measurement.

Protein purification

HT22 cells overexpressing exogenous PDHA1 or mutant PDHA1 were harvested, and lysed proteins were extracted using a mammalian cell and tissue extraction kit (K269-500, BioVision). Anti-Flag beads (B26101, Bimake) were incubated with the cell lysates overnight at 4°C . On the next day, the beads were washed three times with PBST buffer, and the purified proteins were competitively eluted with Flag peptide (B23111, Bimake) and collected for western blotting assay.

Dot blots

The purified peptides were prepared by PTM Biolabs and then provided to PTM Biolabs for the generation of rabbit polyclonal antibodies (PTM Biolabs). For peptide dot blots, the peptides were dotted as progressive protein concentrations on a nitrocellulose membrane. The membranes were left to dry at room temperature for 1 h and then blocked in 5% milk in PBST for 1 h. The immunoreactivity was visualized using a chemiluminescence substrate (WBKLS0500, Millipore) with a chemiluminescence image system (CLINX, Shanghai, China).

LC-MS/MS analysis of protein crotonylation

Protein extraction and trypsin digestion

Samples were sonicated three times on ice using a high-intensity ultrasonic processor (Scientz) in lysis buffer (8 M urea, 1% protease inhibitor cocktail, 3 M TSA, and 50 mM NAM). The remaining debris was removed by centrifugation at 12,000 *g* at 4°C for 10 min. The supernatant was then collected, and the protein concentration was determined with a BCA kit according to the manufacturer's instructions. For digestion, the protein solution was reduced with 5 mM dithiothreitol (DTT) for 30 min at 56°C and alkylated with 11 mM iodoacetamide for 15 min at room temperature in darkness. The protein sample was then diluted by adding 100 mM triethylammonium bicarbonate (TEAB) to urea concentration of less than 2 M. Subsequently, trypsin was added at a trypsin-to-protein mass ratio of 1:50 for the first overnight digestion and at a trypsin-to-protein mass ratio of 1:100 for the second 4-h digestion.

HPLC fractionation

The tryptic peptides were fractionated into fractions by high-pH reversed-phase HPLC using a Thermo BetaSil C18 column (5- μ m particles, ID of 10 mm, length of 250 mm). Briefly, the peptides were first separated using a gradient of 8–32% acetonitrile (pH 9.0) over 60 min into 60 fractions. The peptides were then combined into 10 fractions and dried by vacuum centrifugation.

Kcr peptide enrichment

Tryptic peptides were dissolved in NETN buffer (100 mM NaCl, 1 mM EDTA, 0.5% NP-40 (pH 8.0) and 50 mM tris-HCl) and then incubated with antibody beads at a ratio of 15 μ L beads per milligram of protein at 4°C overnight. The antibody beads were washed four times with NETN buffer and twice with double-distilled H₂O. The Kcr peptides were then eluted by adding elution buffer with 0.1% trifluoroacetic acid. The eluted peptides were cleaned with C18 ZipTips (Millipore) before being subjected to LC-MS/MS analysis.

LC-MS/MS analysis

The tryptic peptides were dissolved in 0.1% formic acid (solvent A) and directly loaded onto a homemade reversed-phase analytical column (length of 15 cm, ID of 75 μ m). The gradient consisted of an increase from 6 to 23% solvent B (0.1% formic acid in 98% acetonitrile) over 26 min, an increase from 23 to 35% over 8 min, and an increase to 80% over 3 min and then maintenance at 80% for the last 3 min, and all of these steps were performed at a constant flow rate of 400 nL/min on an EASY-nLC 1000 ultra performance liquid chromatography (UPLC) system. The peptides were subjected to nanospray ionization source followed by MS/MS with an Q Exactive Plus instrument (Thermo Fisher Scientific) coupled online to the UPLC. The electrospray voltage applied was 2.0 kV. The *m/z* (mass/charge ratio) scan range was 350–1800 for full scan, and intact peptides were detected in the Orbitrap at a resolution of 70,000. The peptides were then selected for MS/MS using a normalized collision energy (NCE) setting of 28, and the fragments were detected in the Orbitrap at a resolution of 17,500. A data-dependent procedure alternated between one MS scan and 20 MS/MS scans with 15.0-s dynamic exclusion. Automatic gain control was set to 5×10^4 . The fixed first mass was set to 100 *m/z*.

Database searching and protein quantification

The resulting MS/MS data were processed using MaxQuant with the integrated Andromeda search engine (v.1.5.2.8). Tandem mass spectra were searched against human Swiss-Prot database (20,203 sequences) concatenated with reverse decoy database. Trypsin/P was specified as the cleavage enzyme, and up to four missing cleavages were allowed. The mass tolerance for precursor ions was set to 20 parts per million in the first search and 5 parts per million in the main search, and the mass tolerance for fragment ions was set to 0.02 Da. Carbamidomethyl on Cys was specified as a fixed modification, and Kcr modification and oxidation on Met were specified as variable modifications. The false discovery rate (FDR) was adjusted to <1%, and the minimum score for modified peptides was set to >40.

Bioinformatics analysis

Motif-X software (<http://motif-x.med.harvard.edu/>) was used to analyze the model of sequences constituted with amino acids in specific positions of Kcr-21-mers (10 amino acids upstream and downstream of the site) in all protein sequences. The minimal number of peptides occurring in one motif "occurrences" was set to 20, and the motif analysis statistics test significance threshold value was set to 0.0000001. The amino acid sequence heatmap is a two-dimensional data matrix in which every row is an amino acid and every column is a position. One cell in the heatmap matrix is colored according to the $\log_{10} p$ value for that position and amino acid, which was calculated using the Fisher's exact test method. The iceLogo (<https://iomics.ugent.be/icelogoserver/>) was used to examine the properties of amino acids surrounding the modification sites based on a *t* test with $p < 0.05$, and the "choosing scoring system" was set to "percentage difference." Secondary structures were predicted using NetSurfP. GO term and KEGG pathway enrichment analyses were performed using the DAVID 6.8. STRING database (<http://string-db.org/>), and protein-protein interactions (PPIs) were analyzed. Cytoscape (version 3.0) software was used to display the network.

QUANTIFICATION AND STATISTICAL ANALYSIS

The number of mice per group and the number of cell experimental are annotated in each of the corresponding figure legends. All data were analyzed using GraphPad Prism 7 software, are presented as the means \pm SEMs, and subjected to the Kolmogorov-Smirnov test to assess the normality of the distribution. For simple comparisons, an unpaired two-tailed Student's *t* test was used. For multiple comparisons, one-way ANOVA or two-way ANOVA, with a repeated-measures factor when necessary, followed by Bonferroni's post hoc tests was utilized for each experiment. In all cases, *n* refers to the number of animals or cell experimental. For all results, $p < 0.05$ was defined as indicating statistical significance.